

Late Quaternary slip rates along the Sierra Nevada frontal fault zone, California: Slip partitioning across the western margin of the Eastern California Shear Zone–Basin and Range Province

Kimberly Le[†]
Jeffrey Lee

Department of Geological Sciences, Central Washington University, Ellensburg, Washington 98926, USA

Lewis A. Owen

Department of Geology, University of Cincinnati, Cincinnati, Ohio 45221, USA

Robert Finkel

Center for Accelerator Mass Spectrometry, Lawrence Livermore National Laboratory, Livermore, California 94550, USA

ABSTRACT

New geologic mapping, tectonic geomorphic, and cosmogenic radionuclide geochronologic data provide the first numerical constraints on late Quaternary vertical slip and horizontal extension rates across the southern Sierra Nevada frontal fault zone, California. This fault zone exposes numerous NNW-striking, east-facing normal fault scarps that offset seven distinct Quaternary alluvial surfaces and a rockslide deposit. Beryllium-10 cosmogenic radionuclide surface-exposure dating of these surfaces provides surface abandonment model ages of 123.7 ± 16.6 ka, 60.9 ± 6.6 ka, 25.8 ± 7.5 ka, 4.4 ± 1.1 ka, and 4.1 ± 1.0 ka on alluvial fan surfaces, and 18.7 ± 3.9 ka on the rockslide deposit. These age constraints, combined with measurements of vertical surface offset across fault scarps, yield preferred late Pleistocene to Holocene vertical and horizontal extensional slip rates of 0.2–0.3 mm/yr and 0.1–0.2 mm/yr. Vertical slip-rate estimates in this study are comparable to late Pleistocene vertical slip-rate estimates across other prominent range-front normal faults within the Basin and Range Province. These geologic and geochronologic results indicate that the eastern escarpment of the southern Sierra Nevada has remained tectonically active throughout the late Quaternary. Combining our data with slip data from the Owens Valley

and Lone Pine faults implies that slip along the eastern escarpment of the Sierra Nevada block is partitioned into three components: dominantly dextral slip along the Owens Valley fault, intermediate oblique slip along the Lone Pine fault, and subordinate normal slip along the Sierra Nevada frontal fault zone. These observations are consistent with global positioning system (GPS) data, which indicate that dextral shear-strain accumulation dominates today along the western boundary of the Eastern California Shear Zone and Basin and Range Province.

Keywords: neotectonics, Sierra Nevada, normal fault, Basin and Range Province, geochronology, Eastern California Shear Zone.

INTRODUCTION

The interaction between continental extension and dextral shear within the southwestern U.S. Cordillera makes it one of the world's best places to examine whether the crust accommodates these different deformation styles by fault-slip partitioning within a single regional stress field or by temporally distinct alternating or cyclic normal and strike-slip stress regimes. One of the most prominent geomorphic features within this region is the Sierra Nevada, a mountain range with a mean elevation of 2800 m above sea level and bounded along its east flank by a normal fault system, the Sierra Nevada frontal fault zone, and a few kilometers farther east by a dextral fault zone, the Owens Valley fault. The Sierra Nevada frontal fault zone and Owens Valley fault define the western boundary

of both the Eastern California Shear Zone and Basin and Range Province, a region where NW dextral shear has been superimposed on E-W extension (Fig. 1).

There is a long history of research on the origin of Sierra Nevada topography and the role the Sierra Nevada frontal fault zone plays in the evolution of this part of the Cordillera (e.g., Lindgren, 1911; Christensen, 1966; Jones et al., 2004). This fault zone was long considered to have formed by regional Basin and Range extension (e.g., Bateman and Wahrhaftig, 1966). More recently, data from global positioning system (GPS), topographic, geoid, and Quaternary fault-slip studies were used to hypothesize that NW dextral shear and E-W extension within the Eastern California Shear Zone resulted from translation of the Sierra Nevada both parallel and perpendicular to the Pacific–North American plate boundary in consequence of plate tractions and gravitational potential energy, respectively (e.g., Flesch et al., 2000; Bennett et al., 2003; Hammond and Thatcher, 2004). Data from petrological, geochemical, and geophysical studies investigating Sierra Nevada lithospheric structure and young deformation along the western boundary of the Basin and Range Province led Jones et al. (2004, and references therein) to suggest that removal of lithosphere beneath the Sierra Nevada at ca. 3.5 Ma initiated uplift and increased extensional strain rates. These authors also postulated that a combination of locally derived internal forces (gravitational potential energy) and plate boundary forces drive fault kinematics along the western boundary of the Eastern California Shear Zone and Basin and Range Province.

[†]Present Address: Department of Geological Sciences, University of North Carolina, Chapel Hill, North Carolina 27599, USA, kle@email.unc.edu.

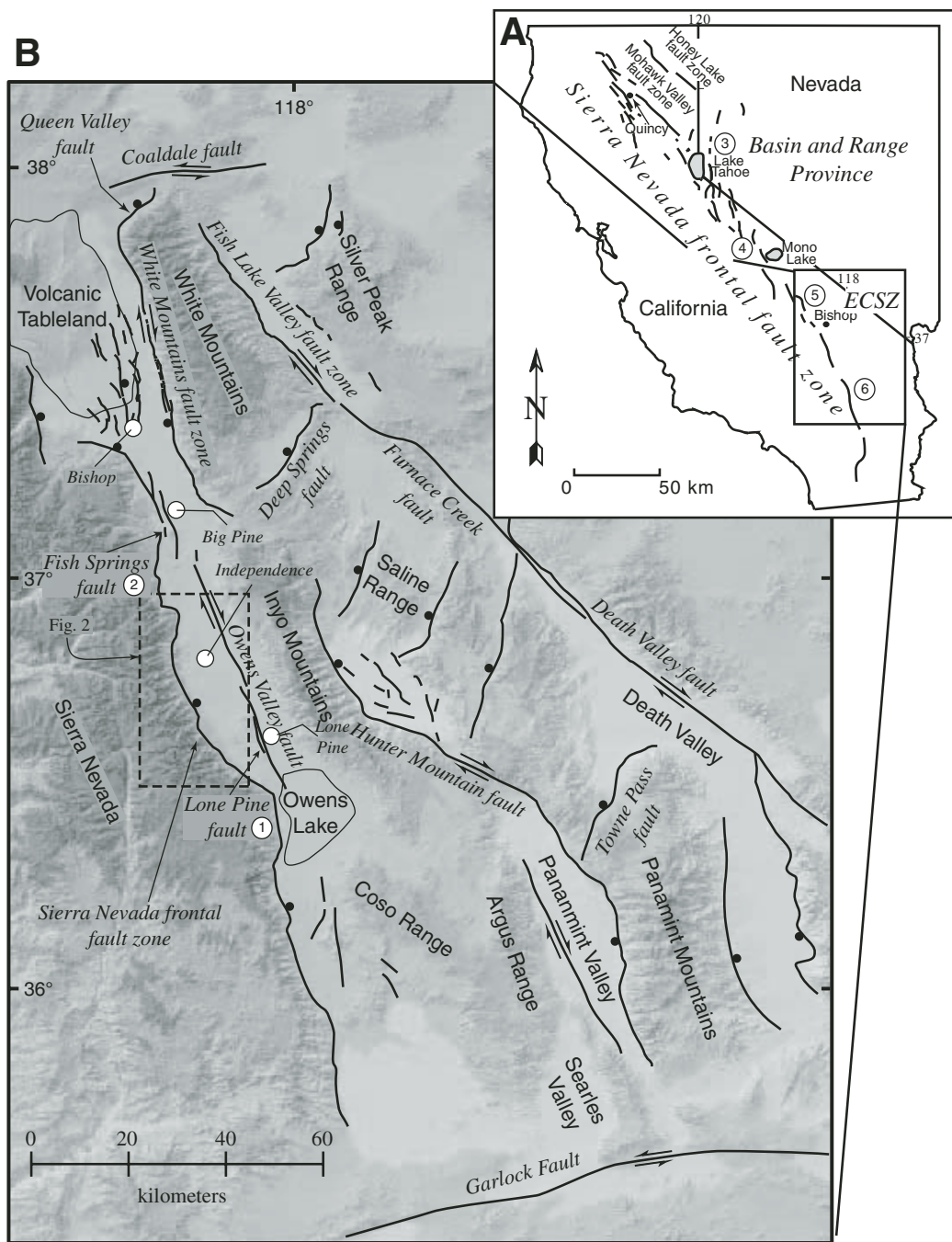


Figure 1. (A) Index map showing location of Sierra Nevada. (B) Shaded relief map of a part of Eastern California Shear Zone (ECSZ) and western Basin and Range Province, showing major Quaternary faults. Solid circles are on the hanging wall of normal faults, and arrows indicate relative motion across strike-slip faults. Circled numbers, keyed to Table 5, show locations of calculated vertical slip rates for the eastern Sierra Nevada range front.

In contrast to these hypotheses, the orientation of normal and strike-slip faults along the eastern margin of the Sierra Nevada relative to the small circles to the Sierra Nevada–North America Euler pole, coupled with kinematic inversions of earthquake focal mechanisms, led Unruh et al. (2003) to hypothesize that most of the normal faulting along the eastern flank of the Sierra Nevada is related to plate-boundary-driven NW translation of this rigid block rather than to Sierra Nevada uplift or Basin and Range extension.

For both hypotheses, motion of the Sierra Nevada block should be accommodated within the upper crust along its eastern flank by either oblique fault slip or spatially partitioned slip into normal and dextral components within a single stress regime, or by temporally partitioned slip into normal and dextral components within alternating normal and strike-slip stress regimes (cf. Wesnousky and Jones, 1994; Bellier and Zoback, 1995). In this paper, we describe the results of new detailed geologic mapping, tectonic, geomorphologic, and cosmogenic

radionuclide (CRN) geochronologic investigations along the southern part of the Sierra Nevada frontal fault zone. Our data provide the first numerical late Quaternary fault-slip rates along this part of the fault zone that bear on how Sierra Nevada motion has been accommodated by fault slip during this time period.

GEOLOGIC SETTING

The Sierra Nevada and the adjacent Central Valley define the rigid Sierran microplate, which

is translating northwest nearly parallel to the relative motion between the Pacific–North American plates (Argus and Gordon, 1991; Dixon et al., 2000). The Sierra Nevada is a west-tilted normal fault block that defines the western margin of both the Eastern California Shear Zone and the Basin and Range Province (Fig. 1). The combination of extensional and dextral shear deformation has resulted in the development of a complex array of NW-striking dextral faults, NE-striking connecting normal faults, and NW-striking, range-bounding normal faults in this part of the Eastern California Shear Zone.

The Sierra Nevada is underlain by Paleozoic and Mesozoic sedimentary and volcanic rocks intruded by Mesozoic granitic rocks, which in turn are overlain by Cenozoic volcanic and sedimentary deposits (Bateman and Wahrhaftig, 1966; Bateman and Eaton, 1967). The Sierra Nevada frontal fault zone forms the eastern escarpment of the Sierra Nevada, extending ~600 km from just north of the Garlock fault to the Cascade Range (Fig. 1), and juxtaposes extensive Quaternary alluvial fan, glacial, and rockslide deposits in the hanging wall upon bedrock in the footwall (Fig. 2). The character of the eastern escarpment of the Sierra Nevada frontal fault zone varies along strike from wide zones of en echelon escarpments to narrow zones characterized by a single escarpment (Fig. 1). South of Bishop, the eastern margin of the Sierra Nevada is defined by a continuous NNW-striking escarpment, whereas from Bishop north to the Lake Tahoe region the escarpment is defined by a series of left-stepping en echelon escarpments that extend some distance from the eastern margin of the Sierra Nevada. North of Lake Tahoe, the eastern margin of the Sierra Nevada is defined by a northward widening zone of NNW-striking, east-dipping en echelon normal faults and dextral faults (Wakabayashi and Sawyer, 2001).

METHODS

Mapping

Geologic mapping of fault-related features such as fault lineations, fault scarps, triangular facets, steep linear range fronts, wine glass canyons, and alluvial aprons, and of different Quaternary alluvial fan surfaces, using cross-cutting relations and surface morphology, was completed on 1:15,000-scale color aerial photographs. Alluvial fans along the eastern piedmont of the Sierra Nevada have been subjected to multiple episodes of glacial, debris, and stream deposition. These episodes bear on the development of fan size, height, slope, and surface morphology, allowing for different stages of deposition to be identified.

Fan units were differentiated on the basis of surface morphology, including the presence or absence of bar and swale morphology, degree of fan dissection, weathering of granite boulders, color, slope, and terrace height and inset geometry. On the basis of geologic mapping, selected sites were chosen for CRN geochronological studies and topographic profiling across fault scarps of vertically offset geomorphic features to define the age of surface abandonment and vertical fault-slip rates.

Cosmogenic Radionuclide (CRN) Dating

CRN geochronological studies constrain the age of abandonment of each alluvial surface,

which, combined with measured vertically offset alluvial surfaces, allow calculation of vertical slip rates across normal fault scarps. CRN geochronology measures the amount of nuclides produced in the rock by cosmic ray bombardment (Kohl and Nishiizumi, 1992; Gosse and Phillips, 2001; Muzikar et al., 2003).

Samples collected for CRN geochronology must satisfy several criteria (Gosse and Phillips, 2001). One criterion is that the surface or boulder sampled has been in its original position since first being exposed to cosmic radiation, with no inheritance or prior exposure of the sampled surface. Inheritance, or prior exposure of sampled surfaces, can yield older surface exposure ages than the actual date of abandonment. In contrast

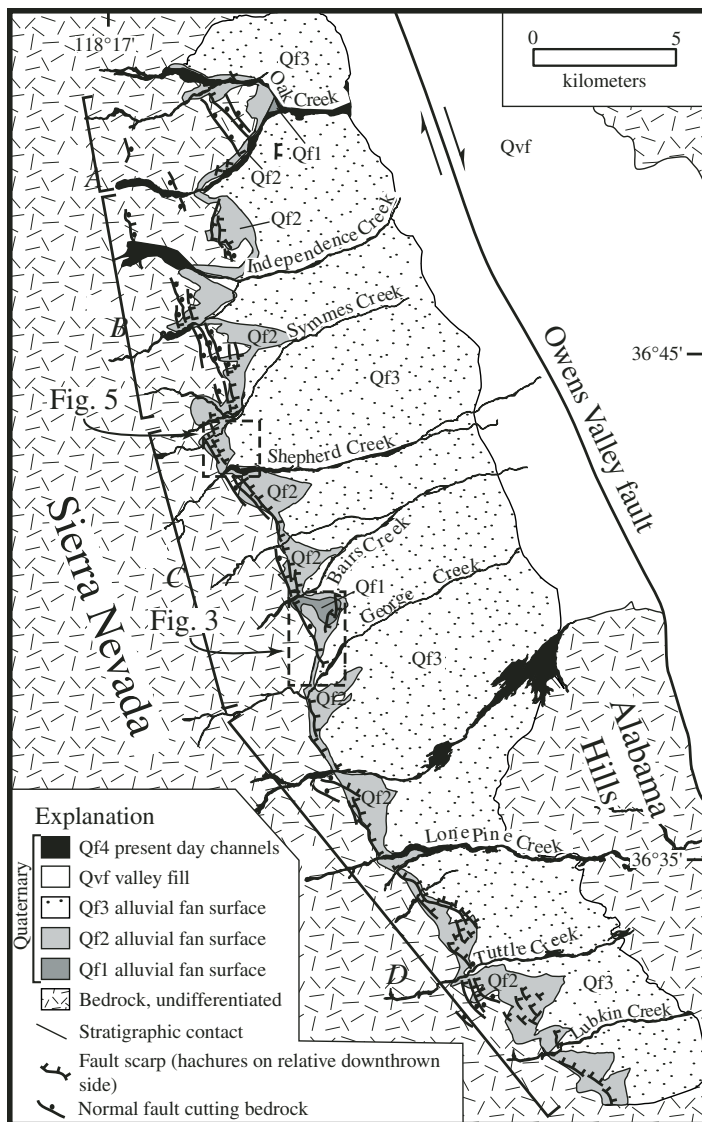


Figure 2. Simplified geologic map along the southern Sierra Nevada frontal fault zone, showing major normal-fault scarps cutting Quaternary alluvial fan surfaces. Location shown in Figure 1.

to inheritance, erosion or exhumation of the boulder surface can attenuate the concentration of cosmogenic isotopes, thus reducing the true exposure age of a boulder (Gosse and Phillips, 2001). In addition, factors such as erosion and weathering can reduce the concentration of cosmogenic radionuclides as the boulders progressively denude with time. To alleviate these potential problems, we sampled five boulders from each surface to constrain the age of abandonment of that surface.

The uncertainties associated with ^{10}Be exposure ages are summarized in Gosse and Phillips (2001). Some of these uncertainties include the reliability of the production rate (9%), assumptions associated with model ages (3%), analytical and sample preparation errors (3%), and latitude, longitude, and altitude scaling errors (5%). Surface-exposure ages were corrected for 0.3 cm/k.y. (Small et al., 1997) of boulder surface erosion. The reliability of our model surface-exposure ages therefore relies on the assumed production rates, erosion rate estimates, and the geologic error associated with ^{10}Be CRN ages.

Samples of ~300–1000 g were collected from the top 1–5 cm of each boulder, using a rock hammer and chisel. Boulders were selected from localities where there was little or no apparent evidence of boulder exhumation. Sample sites were recorded on aerial photographs, using a Garmin GPS receiver to locate the position of each sample site to within ~10 m. Once collected, samples were crushed, ground, pulverized, and sieved to a grain size of 250–500 μm .

A leaching procedure of 1 part water to 2 parts HF was used to purify the quartz and to remove meteoric ^{10}Be (Kohl and Nishiizumi, 1992). Beryllium carrier was then added to the sample as it was dissolved in HF, and Be was separated by ion exchange chromatography (Kohl and Nishiizumi, 1992). Beryllium was then precipitated as the hydroxide and converted to beryllium oxide by ignition in quartz at 750 °C (Kohl and Nishiizumi, 1992; Gosse and Phillips, 2001). The oxide was mixed with niobium powder prior to determination of ^{10}Be , using the Lawrence Livermore National Laboratory Center for Accelerator Mass Spectrometry FN tandem van de Graaff accelerator mass spectrometer. ^{10}Be was determined relative to standards prepared from an ICN ^{10}Be solution by K. Nishiizumi, using a ^{10}Be half-life of 1.5×10^6 yr.

The measured isotope ratios were converted to radionuclide concentrations in quartz, using the total Be in the samples and the sample weights. Age determinations were calculated with a sea-level, high-latitude (SLHL) production rate of 5.44 at/g-quartz, using scaling factors in Lal (1991) as modified by Stone (2000) with a

SLHL production by muons accounting for 3% of the total. A correction for variation in the geomagnetic field was applied to determine the final age of each sample as described in Nishiizumi et al. (1989), using the SINT800 geomagnetic intensity assessment. The topographic and depth corrections were performed by numeric integration of the flux for the dip and topography-corrected elevation at all azimuth directions.

^{10}Be model age results for 25 samples collected from five alluvial fan surfaces and a rockslide are summarized in Table 1; sample localities are shown in Figures 3–6.

Fault Scarp Measurement

Global positioning system (GPS) precise point kinematic (PPK) surveys, using dual frequencies L1/L2 GPS receivers, were employed to measure the vertical offset of alluvial fan surfaces across normal fault scarps. Twenty-two topographic profiles were measured perpendicular to NNW-striking, E-facing fault scarps, which cut distinct alluvial fan surfaces along the eastern Sierra Nevada escarpment. Topographic profiles were measured on fault scarps developed in unconsolidated alluvial deposits, and across which material is transported down fault-scarp dip by rain splash and soil creep processes, but not in or out of the profile (McCalpin, 1996; Arrowsmith et al., 1998). Data collected during each survey were downloaded, using the Trimble Geomatics Office and corrected for changes in the geoid height and reprojected into the reference frame North American Datum 83, zone 11. Maximum vertical offsets of alluvial surfaces were calculated geometrically, using the middle of the fault scarp (Fig. 7). Errors associated with the vertical offset measurements include surface roughness (~20 cm) and GPS survey points (≤ 10 cm). Because the larger of the two errors is <5% of the measured vertical offset, we report a conservative error of 5%, which is smaller than the error associated with CRN ages.

ROCK UNITS AND AGES

The southern escarpment of the Sierra Nevada frontal fault zone, between Oak and Lubkin Creeks, offsets granite- and metamorphic-derived Quaternary coarse- to fine-grained alluvial fan, glacial, and rockslide deposits (Figs. 2–6). We mapped seven Quaternary alluvial fan surfaces of distinct ages on the basis of surface morphology, terrace height, and inset geometry, and moraine and rockslide deposits. Twenty-five quartz-rich granite boulder samples were collected for model CRN ^{10}Be exposure age dating of these surfaces; ^{10}Be model ages reported in this study are recalculated, assuming

an erosion rate of 0.3 cm/k.y. of the boulder surface (Small et al., 1997) (Table 1).

At the apex of drainage basins along the eastern range front of the Sierra Nevada, remnants of the oldest alluvial surfaces, Qf1, typically appear as 30–100-m-high mounds (Figs. 3 and 4). Qf1 surfaces are orange to orange-tan in the field and on aerial photographs, and are partly varnished, highly dissected, and strongly weathered with scarce, typically strongly weathered elephant-skin boulder deposits. Surfaces consist of weathered residual fragments of granitic rocks, such as rounded to subrounded clasts of cobbles and pebbles, intermixed in a coarse and brittle grus and sand matrix (Fig. 8A). Model ^{10}Be ages for boulder samples collected from an offset Qf1 surface just south of Bairs Creek yielded a mean surface exposure age of 123.7 ± 16.6 ka (Table 1; Fig. 3).

Based on the degree of surface dissection and inset geometry, Qf2 surfaces, constituting the next youngest surface, have been subdivided into two surfaces. Older Qf2a surfaces are characterized by a ridge and ravine topographic pattern, typically yellow to yellow-tan on aerial photographs, and are slightly varnished, highly dissected (ranging from a few meters to tens of meters above the modern channel), moderately vegetated, and best characterized by their lack of boulders (Figs. 4 and 6). Qf2a surfaces are typically underlain by unconsolidated fan deposits composed primarily of weathered coarse angular to subangular grus.

Younger Qf2b alluvial surfaces are inset into and exhibit features similar to Qf2a surfaces. However, Qf2b surfaces lack a well-developed ridge and ravine topographic pattern, and are moderately dissected, hummocky, and less weathered than Qf2a alluvial surfaces (Figs. 4, 6, and 8B). In addition, some Qf2b surfaces are overlain by moderately weathered granitic boulders that make up to 2% of the alluvial surface. Qf2b alluvial surfaces adjacent to drainages generally contain higher boulder abundances in comparison with Qf2b surfaces distal from drainages. Loose, subangular granitic pebbles, cobbles, and sand grus typically characterize the deposits that underlie these surfaces. The mean ^{10}Be model age calculated for the Qf2b surface just north of Symmes Creek is 60.9 ± 6.6 ka (Table 1; Fig. 5).

The areally dominant alluvial fan deposits along the range front are Qf3 deposits (Fig. 2). Based on the plumose texture caused by the topographic patterns of bars and swales, along with inset geometry, Qf3 surfaces have been subdivided into three units: Qf3a, Qf3b, and Qf3c. The oldest surfaces, Qf3a, are typically yellow-tan to tan-white on aerial photographs, planar, densely vegetated, and exhibit weakly developed desert

TABLE 1. SUMMARY OF ¹⁰Be MODEL AGES

| Sample number | Latitude (N) | Longitude (W) | Altitude (m) | Depth and topography correction | ¹⁰ Be measured (10 ⁹ atom g ⁻¹) | No erosion ¹⁰ Be age (ka) [†] | Error [‡] ± | Erosion ¹⁰ Be age (ka) [§] | Error [‡] ± |
|---------------------------------------|--------------|---------------|--------------|---------------------------------|---|---|----------------------|--|----------------------|
| Fan Surface, Qf1 | | | | | | | | | |
| K20 | 36°41.629 | 118°14.777 | 1887 | 0.96 | 1.78 ± 0.044 | 87.5 | 2.2 | 106.5 | 2.6 |
| K21 | 36°41.626 | 118°14.778 | 1887 | 0.96 | 2.20 ± 0.055 | 107.3 | 2.7 | 139.7 | 3.5 |
| K22 | 36°41.630 | 118°14.763 | 1890 | 0.99 | 2.10 ± 0.057 | 99.4 | 2.7 | 125.0 | 3.4 |
| K23 [#] | 36°41.607 | 118°14.792 | 1893 | 0.96 | 1.43 ± 0.043 | 69.4 | 2.1 | 81.8 | 2.5 |
| K24 [#] | 36°41.627 | 118°14.776 | 1884 | 0.97 | 1.27 ± 0.041 | 69.8 | 2.0 | 69.4 | 2.3 |
| Mean age ±1 standard deviation | | | | | | 98.1 ± 10.0 | | 123.7 ± 16.6 | |
| Fan Surface, Qf2b | | | | | | | | | |
| K2 [#] | 36°43.848 | 118°16.482 | 1869 | 0.97 | 1.53 ± 0.036 | 74.7 | 1.8 | 89.2 | 2.1 |
| K3 | 36°43.781 | 118°16.488 | 1871 | 0.96 | 0.96 ± 0.031 | 46.7 | 1.5 | 53.4 | 1.7 |
| K4 [#] | 36°43.851 | 118°16.486 | 1873 | 0.99 | 0.44 ± 0.017 | 22.2 | 0.8 | 23.1 | 0.9 |
| K5 | 36°43.821 | 118°16.414 | 1859 | 0.96 | 1.17 ± 0.038 | 58.0 | 1.9 | 66.0 | 2.2 |
| K6 | 36°43.825 | 118°16.408 | 1859 | 0.96 | 1.12 ± 0.040 | 55.5 | 2.0 | 63.2 | 2.3 |
| Mean age ±1 standard deviation | | | | | | 53.4 ± 6.0 | | 60.9 ± 6.6 | |
| Fan Surface, Qf3a | | | | | | | | | |
| K12 | 36°43.245 | 118°16.104 | 1881 | 0.98 | 0.71 ± 0.009 | 34.3 | 0.8 | 36.6 | 0.8 |
| K13 | 36°43.198 | 118°16.091 | 1895 | 0.98 | 0.45 ± 0.002 | 22.4 | 0.5 | 23.5 | 0.5 |
| K14 | 36°43.159 | 118°16.096 | 1903 | 0.98 | 0.34 ± 0.002 | 17.0 | 0.4 | 17.6 | 0.5 |
| K15 | 36°43.158 | 118°16.067 | 1901 | 0.99 | 0.58 ± 0.003 | 28.2 | 0.9 | 29.9 | 0.9 |
| K16 | 36°43.154 | 118°16.062 | 1900 | 0.98 | 0.41 ± 0.009 | 20.4 | 0.5 | 21.2 | 0.5 |
| Mean age ±1 standard deviation | | | | | | 24.5 ± 6.8 | | 25.8 ± 7.5 | |
| Fan Surface, Qf3c | | | | | | | | | |
| K7 | 36°43.835 | 118°16.357 | 1852 | 0.98 | 1.08 ± 0.003 | 5.9 | 0.2 | 6.0 | 0.2 |
| K8 | 36°43.776 | 118°16.285 | 1853 | 0.97 | 0.70 ± 0.003 | 4.1 | 0.2 | 4.1 | 0.2 |
| K9 | 36°43.776 | 118°16.285 | 1853 | 0.98 | 0.51 ± 0.003 | 3.1 | 0.2 | 3.1 | 0.2 |
| K10 | 36°43.821 | 118°16.275 | 1846 | 0.99 | 0.67 ± 0.001 | 3.7 | 0.6 | 3.7 | 0.6 |
| K11 | 36°43.802 | 118°16.225 | 1847 | 0.97 | 0.85 ± 0.004 | 4.9 | 0.2 | 5.0 | 0.2 |
| Mean age ±1 standard deviation | | | | | | 4.3 ± 1.1 | | 4.4 ± 1.1 | |
| Fan Surface, Qf4 | | | | | | | | | |
| K17 | 36°43.121 | 118°14.886 | 1726 | 0.98 | 0.61 ± 0.002 | 3.9 | 0.2 | 4.0 | 0.2 |
| K18 | 36°43.119 | 118°14.903 | 1727 | 0.98 | 0.67 ± 0.002 | 4.3 | 0.1 | 4.3 | 0.1 |
| K19 | 36°43.119 | 118°14.903 | 1727 | 0.98 | 0.62 ± 0.003 | 4.0 | 0.2 | 4.0 | 0.2 |
| Mean age ±1 standard deviation | | | | | | 4.1 ± 1.0 | | 4.1 ± 1.0 | |
| Rockslide | | | | | | | | | |
| K1 | 36°48.216 | 118°18.554 | 2164 | 0.98 | 0.38 ± 0.009 | 15.4 | 0.1 | 15.9 | 0.1 |
| K105 | 38°48.215 | 118°18.551 | 2167 | 0.98 | 0.49 ± 0.046 | 20.5 | 0.2 | 21.4 | 0.2 |
| Mean age ±1 standard deviation | | | | | | 18.0 ± 3.6 | | 18.7 ± 3.9 | |

[†]¹⁰Be model ages without accounting for erosion.

[‡]Error reported is analytical.

[§]¹⁰Be model ages accounting for 0.3 cm/k.y. of erosion.

[#]Boulder samples that are not used in the calculation of mean owing to exhumation or inheritance.

varnish (Figs. 4 and 6). Large boulders are rare, making up <1% of the alluvial surface, and some are embedded into the alluvial surface. These surfaces typically contain a *grus* matrix of finer-grained residual granite clasts (Fig. 8C). Boulder samples collected from a Qf3a alluvial surface ~1 km east of the range front and just north of Shepherd Creek yield a mean ¹⁰Be model age of 25.8 ± 7.5 ka (Table 1; Fig. 5).

The next youngest fan surface, Qf3b, extends up to 11 km from the range front, farther than any other alluvial fan surface (Figs. 3, 4, 5, and 6). Inset into Qf3a surfaces, Qf3b surfaces consist of moderately muted bar and swale morphology and are best distinguished by the incision of dendritic channel networks, which range from

1.0 to 2.5 m deep, and include granitic boulders (Whipple and Dunne, 1992). Hummocky surface morphology characterizes the proximal surfaces, whereas distal surfaces are smooth surfaces with low surface relief of 0 to 3°. Qf3b surfaces are typically covered with boulders averaging 1–3 m high, composing ~5% of the surface and locally up to 50% on linear levees (Fig. 8D). The clasts on Qf3b surfaces contain subangular to subrounded granitic boulders, cobbles, and pebbles in a coarse-grained sand matrix.

The youngest Qf3 surface, Qf3c, extends ~2–4 km from the range front and exhibits well-preserved bar and swale morphology (Figs. 3–6). Fan surfaces are undissected, unvarnished, and hummocky, and contain many boulder-lined

channels. Boulder clasts are fresh, range in size from ~1 to ~9 m high, and constitute up to ~20% of the alluvial surface, suggesting glacial-outburst flood deposition (Blair, 2001) (Fig. 8E). Samples collected from a Qf3c fan surface at the mouth of Symmes Creek and just south of the modern channel yield a mean ¹⁰Be surface exposure age of 4.4 ± 1.1 ka (Table 1; Fig. 5).

The youngest surface, Qf4 deposits, cuts all other surfaces and consists of active channels inset into recently abandoned channels (Figs. 3–6). These surfaces contain recent debris-flow deposits, which include tree trunk clasts and boulder levee bars, and are densely vegetated. The boulders on Qf4 surfaces are typically unvarnished, suggesting recent

deposition. Boulder samples collected from a Qf4 surface above the modern channel of Shepherd Creek on a recent debris flow, consisting of dead trees intermixed with boulder debris, yield a mean ^{10}Be model age of 4.1 ± 1.0 ka (Table 1; Fig. 5).

Exposed along the range front northwest of Independence Creek and north of Onion Valley Road is a large ~ 1 km² rockslide deposit, Qrs, characterized by hummocky surface morphology and deposits of large (>0.5 m), angular granitic boulders with no matrix (Fig. 8f). The ^{10}Be model age for the abandonment of the rockslide is 18.7 ± 3.9 ka (Table 1).

Moraine deposits, Qm, that bound Onion Creek form narrow, elongated lobes of glacially transported sediment overlain by large granitic boulders (ranging from ~ 1 to >8 m high) along the crest of the lobe.

A number of studies suggested that alluvial fan deposition along the eastern flank of the Sierra Nevada is associated with glacial events (Gillespie, 1982; Bierman et al., 1995). Our model ^{10}Be erosion ages for alluvial fan surfaces agree, within error, with the timing of glacial events in the Sierra Nevada and continental glaciation (Table 2), thus confirming these earlier studies. The exceptions are Qf3c and Qf4 surfaces, which contain levee boulder bars, suggesting that they are debris-flow deposits rather than glacially related. In addition, our model surface exposure ages agree, within error, with model surface abandonment ages of alluvial fan surfaces elsewhere along the Sierra Nevada range front (Bierman et al., 1995; Zehfuss et al., 2001) (Table 2). These correlations support our assessment that the calculated ^{10}Be model ages can be reliably used to constrain the timing of fan abandonment and thereby provide a geochronologic marker to calculate vertical slip rates across fault scarps.

FAULT GEOMETRY, MAGNITUDE OF OFFSET, AND SLIP RATES

Our study of the Sierra Nevada frontal zone, which we define as the fault zone composed of multiple fault scarps along the eastern piedmont of the Sierra Nevada, centered on an ~ 35 -km-long and up to ~ 5 -km-wide section between Oak and Lubkin Creeks (Fig. 2). This part of the Sierra Nevada frontal fault zone is characterized by NNW-striking, dominantly E-dipping, with lesser W-dipping, normal fault scarps that typically juxtapose Quaternary sediment in the hanging wall upon either Quaternary sediment or granite bedrock in the footwall. The fault scarps cut and offset Qf1, Qf2, and Qf3 surfaces, and the rockslide and glacial moraine deposits, but not Qf4 surfaces. On the basis of

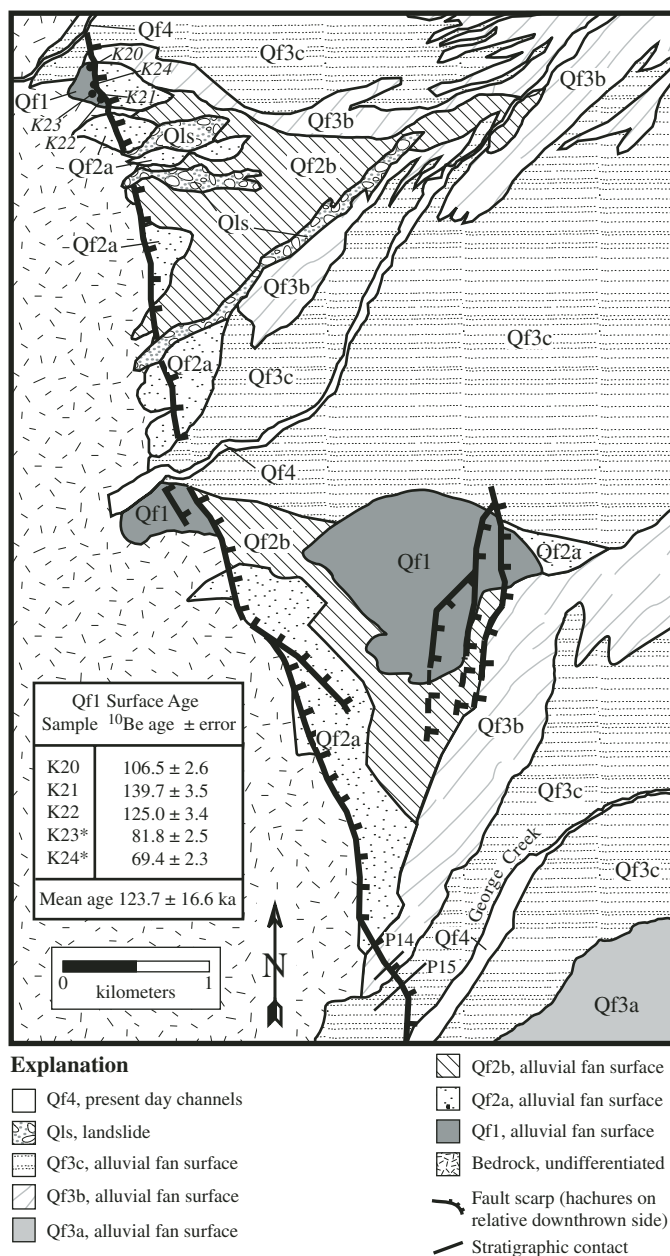


Figure 3. Detailed geologic map of the George Creek area, showing normal-fault scarps cutting alluvial fan surfaces, location of Qf1 cosmogenic radionuclide samples, and two topographic profiles (P14 and P15) across surfaces Qf3b and Qf3c. Box shows calculated ^{10}Be boulder age for each sample and mean age for the Qf1 surface; asterisk (*) indicates boulder sample age not calculated in the mean. Ages incorporate an erosion rate of 0.3 cm/k.y. Location shown in Figure 2.

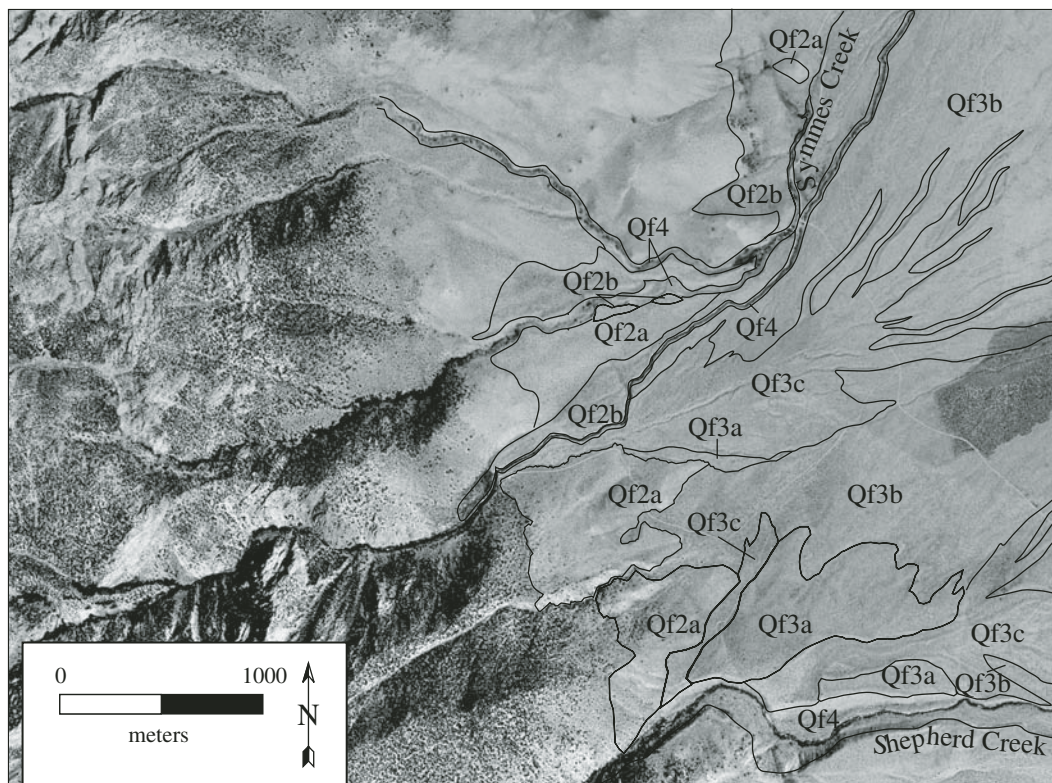


Figure 6. Aerial photograph of the area of Symmes and Shepherd Creeks, highlighting different alluvial fan surfaces. See Figure 5 for a detailed geologic map of the region.

fault zone width, geometry, and strike, this part of the Sierra Nevada frontal fault zone can be subdivided into four distinct, right-stepping segments, A–D (Fig. 2). Faults that define each segment have an average strike of $\sim 334^\circ$, whereas faults that define the step-over between segments have an average strike of $\sim 10^\circ$. Segment A, a 4-km-long and 4-km-wide zone, consists of six subparallel, NW-striking, E-dipping normal faults. South of segment A, the locus of faulting steps ~ 1 km to the west to segment B, a 7-km-long and 5-km-wide zone dominated by as many as seven subparallel NNW-striking, E- and W-dipping, W-stepping en echelon normal faults. Segment C, in the central part of the map area, is ~ 10 km long and ~ 2 km wide and consists of four subparallel, E-dipping en echelon normal faults. Faulting steps ~ 1 km westward to the south into segment D, an ~ 12 -km-long and

~ 2 -km-wide zone of NNW-striking, E-dipping normal faults. Debris-flow levees offset across the Sierra Nevada frontal fault zone exhibit only dip-slip motion. This observation, combined with no evidence for laterally offset alluvial fan surfaces, indicates that this fault zone records only dip slip.

Direct measurements of vertically offset alluvial fan surfaces across fault scarps define the amount of Quaternary vertical displacement. In turn, these measurements, combined with numerical ages on the surfaces, allow us to calculate vertical slip rates averaged over many seismic cycles along this section of the Sierra Nevada frontal fault zone. Twenty-two topographic profiles were measured perpendicular to east-facing fault scarps, which cut and offset distinct alluvial fan surfaces. Locations of representative topographic profiles are shown in

Figures 3–5, representative profiles are shown in Figure 9, and results are listed in Table 3.

Most scarps are moderately eroded and degraded, and sparsely to moderately vegetated (Fig. 10). Measurements across fault scarps yield vertical-surface offset measurements that range from 41.0 ± 2.0 m to 2.0 ± 0.1 m (Table 3; Fig. 9). Topographic profiles P4, P6, and P12 (Figs. 3 and 5) were measured across offset alluvial surfaces for which we determined model ^{10}Be CRN ages (Table 1).

The most prominent fault scarp is an exhumed and eroded granite bedrock fault plane ~ 500 m north of Tuttle Creek (Figs. 2 and 10A). This $\sim N37^\circ\text{W}$ -striking and $\sim 51^\circ\text{NE}$ -dipping fault juxtaposes Quaternary alluvium in the hanging wall upon granitic bedrock in the footwall; topographic profiling yields a minimum vertical offset of 130.0 ± 6.5 m across the fault.

Exposures of Qf1 surfaces are uncommon; therefore, the preserved offset of Qf1 was found in only two localities (Fig. 2). Minimum vertical-surface offset measurements of Qf1 range from 12.5 ± 0.6 m to 40.8 ± 2.0 m, and fault-scarp angles range from 14° to 25° (Table 3).

At the mouths of most creeks and canyons, Qf2a surfaces are cut by a series of subparallel, NNW-striking, E-dipping normal faults. Topographic profiles measured across these fault scarps yield vertical offsets that range from 14.7 ± 0.7 m to 41.0 ± 2.1 m, and

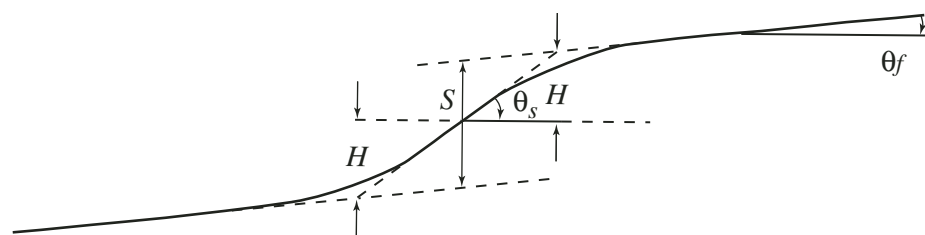


Figure 7. Geometry of an idealized fault scarp, after Hanks et al. (1984). $2H$ —scarp height; S —surface offset or scarp offset; θ_f —far-field slope angle; θ_s —scarp slope angle.

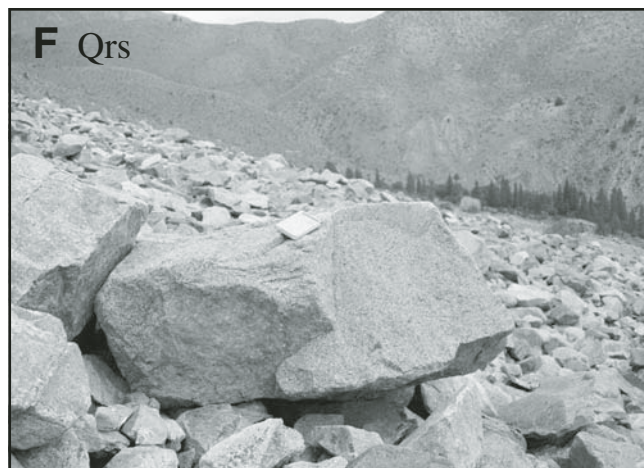
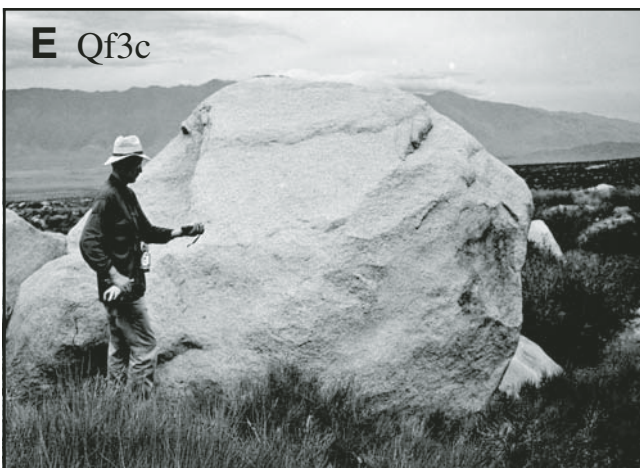
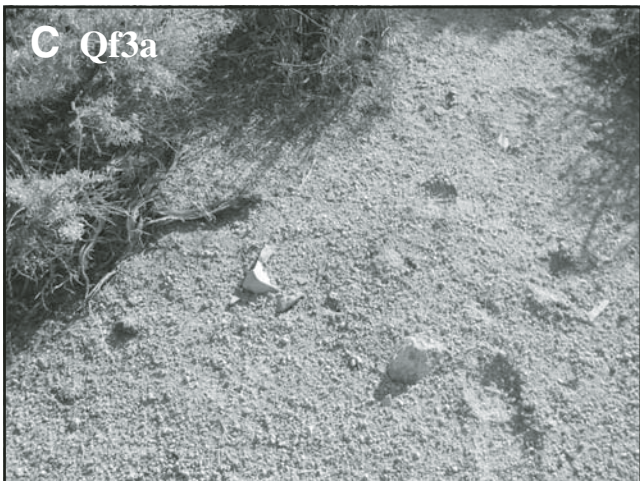
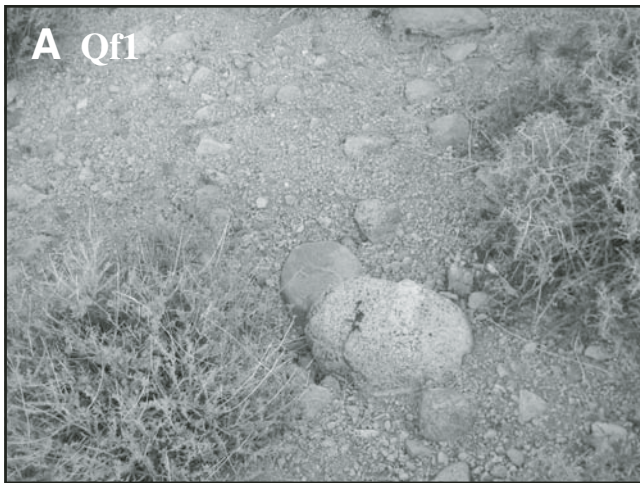


Figure 8. Field photographs of typical alluvial fan surfaces: (A) Qf1, (B) Qf2b, (C) Qf3a, (D) Qf3b, (E) Qf3c, and (F) Qrs.

TABLE 2. POST-SHERWIN GLACIAL CHRONOLOGIES AND ALLUVIAL FAN SURFACE-EXPOSURE AGES OF THE SOUTHERN SIERRA NEVADA

| Glacial event | Relative age | | | Numerical age | | |
|---------------------|------------------|------------------------|----------------------------|------------------------------------|------------------------------------|--|
| | Gillespie (1982) | Phillips et al. (1990) | Marine isotope stage (age) | Bierman et al. (1995) [†] | Zehfuss et al. (2001) [‡] | This study (alluvial surface) [‡] |
| Tioga | 11–25 ka | 21–23 ka | Stage 2 (13–32 ka) | 12 ± 4 | 15 ± 1/13 ± 1 | 19 ± 4 ka (Qrs) |
| Tenaya | 35–45 ka | 24–26 ka | Stage 2 (13–32 ka) | 25 ± 6.0 | — | 26 ± 8 ka (Qf3a) |
| Tahoe/Younger Tahoe | 65–90 ka | 43–50 ka | Stage 4 (64–75 ka) | — | — | 61 ± 7 ka (Qf2b) |
| Mono Basin | 130 ka | 103–119 ka | Stage 6 (128–195 ka) | 98 ± 30.1 | 136 ± 17 | 124 ± 17 ka (Qf1) |

[†]¹⁰Be model age, no erosion.
[‡]¹⁰Be model erosion age.

fault-scarp-slope angles that range from 11° to 18° (Fig. 9; Table 3). Topographic profiles measured across normal fault scarps that cut Qf2b surfaces yield vertical offsets that range from 8.7 ± 0.4 m to 23.9 ± 1.2 m, and fault-scarp-slope angles that range from 16° to 24° (Figs. 9 and 10B; Table 3).

Two Qf3a surfaces have vertical offsets of 6.4 ± 0.3 and 10.2 ± 0.5 m, with fault-scarp-slope angles of 21° to 22° (Figs. 9 and 10C; Table 3). Topographic profiles across prominent fault scarps that offset Qf3b fan surfaces yielded fault scarp slope angles between 18° to 33° and a vertical offset range of 5.0 ± 0.3 m to 6.4 ± 0.3 m. A profile across a fault scarp that cuts Qf3c yields a vertical offset of 6.9 ± 0.3 m (Fig. 9; Table 3). The magnitude of vertical offset of Qf3b and Qf3c surfaces is similar, suggesting that this episode of faulting initiated after abandonment of both surfaces. We suggest that the offset Qf3c surface just north of George Creek (Figs. 3 and 4) is slightly older than the dated Qf3c surface at Symmes Creek (Figs. 5 and 6), because it is the only Qf3c surface with documented displacement.

Finally, a topographic profile measured just south of the Qrs unit east of Onion Valley Road yields a vertical displacement of 3.7 ± 0.2 m and a fault-scarp-slope angle of ~25° (Table 3).

Combining data from ¹⁰Be CRN surface-exposure model ages of offset alluvial fan surfaces with vertical offset measurements across fault scarps (maximum, weighted mean, and dated surface vertical offset values) yields vertical slip-rate estimates of 0.2–0.3 ± 0.1 mm/yr since ca. 124 ka, 0.2–0.4 ± 0.1 mm/yr since ca. 61 ka, 0.3–0.4 ± 0.2 mm/yr since ca. 26 ka, and 1.6 ± 0.4 mm/yr since ca. 4 ka (Table 4). Linear regressions through age versus vertical offset plots yield average late Pleistocene to Holocene vertical slip rates of 0.2–0.3 mm/yr (Fig. 11). Because the average vertical slip-rate values are the same, within error, as calculated slip rates for single time periods (cf. Table 4), the average is our preferred rate. If the calculated average vertical slip rate was constant through time, then the linear regressions suggest that undated surfaces

Qf2a and Qf3b were abandoned at ca. 112–115 ka and 3.3–7.5 ka, respectively. We assume that a fault dip of 60° yields calculated horizontal extension rates for the late Pleistocene to Holocene that range from 0.1 to 0.2 ± 0.1 mm/yr to 0.9 ± 0.4 mm/yr (Table 4). Our calculated late Holocene vertical and horizontal slip rates of 1.6 ± 0.4 mm/yr and 0.9 ± 0.4 mm/yr, respectively, are 2 to 20 times faster than our late Pleistocene and calculated average estimates. This indicates either that horizontal extension rates have increased over the last 4,000 yr, that these calculated slip rates are maxima because these faults are early in the earthquake cycle, or that the ~7 m offset is the result of two or more earthquakes clustering in time. The third hypothesis implies that long-term slip rates vary over short time scales of 100–10,000 yr, resulting in a short-term increase in slip velocities that increases both strain accumulation and resulting release during that period (Rockwell et al., 2000; Peltzer et al., 2001).

DISCUSSION

Vertical Slip Rates and Regional Tectonics

Our preferred late Pleistocene to Holocene vertical slip-rate estimates of 0.2–0.3 mm/yr are the first based on numerical ages for offset geologic markers along the southern Sierra Nevada frontal fault zone. Our late Pleistocene to Holocene slip-rate determinations are the same, within uncertainty, as geologic slip rates based on relative age estimates of offset geologic markers for the southern and central parts of the Sierra Nevada frontal fault zone (Clark, 1972; Gillespie, 1982; Berry, 1989; Clark and Gillespie, 1993) (Table 5). For the Lone Pine fault, exposed ~10 km east of the field area, offset measurements (Lubetkin and Clark, 1988; Beanland and Clark, 1994) and ¹⁰Be CRN model exposure ages of 11.6 ± 3.7 ka on granitic boulders from the offset surface (Bierman et al., 1995) yield a Holocene vertical slip rate of 0.5 ± 0.2 mm/yr—the same, within error, as our late Pleistocene to Holocene estimate. Likewise, for

the Fish Springs fault, exposed to the NNE of our map area (Fig. 1), fault offset measurements and ¹⁰Be CRN model exposure ages on offset alluvial surfaces yielded a late Pleistocene vertical slip rate of ~0.2 mm/yr (Zehfuss et al., 2001) (Table 5). Vertical offset measurements across normal fault scarps and ¹⁴C and optically stimulated luminescence dating of deformed sediments within the Lake Tahoe basin yielded late Pleistocene vertical slip rates of 0.4–0.9 mm/yr (Kent et al., 2005), which are somewhat higher than our estimates (Table 5).

The absence of Cenozoic rocks that can be correlated across the Sierra Nevada and into Owens Valley precludes a direct comparison of our short-term slip rates with long-term slip rates for this section of the Sierra Nevada frontal fault zone. The nearest units that can be correlated across the fault zone are exposed to the northwest at the headwaters of the San Joaquin River. Here, a 2.2–3.6 Ma volcanic unit is vertically separated by ~980 m across the fault zone (Wakabayashi and Sawyer, 2001), implying a long-term vertical slip rate of 0.3–0.4 mm/yr, the same, within error, as our vertical slip-rate estimates. Farther north, late Miocene to early Pliocene units are vertically separated by 600–1100 m (Wakabayashi and Sawyer, 2001), implying a long-term vertical slip rate of 0.1–0.2 mm/yr, the same as our estimates. Geophysical data across Owens Valley suggest that the piedmont between the Sierra Nevada frontal fault zone and the Alabama Hills (Fig. 2) is underlain by a ~100-m-thick sequence of alluvial fan deposits upon bedrock (Pakiser et al., 1964). If our preferred late Pleistocene to Holocene vertical slip rates have remained constant through time, then the eastern escarpment here may be as old as 9–14 Ma, considerably older than the proposed Pliocene (ca. 5.0–3.5 Ma) tectonic uplift of the Sierra Nevada (e.g., Wakabayashi and Sawyer, 2001; Jones et al., 2004). One potential explanation for this discrepancy is that vertical slip rates were higher in the past; a reduction in erosion rates since ca. 1.5 Ma for several rivers in the southern Sierra Nevada (Stock et al., 2004) supports such an interpretation. Alternatively,

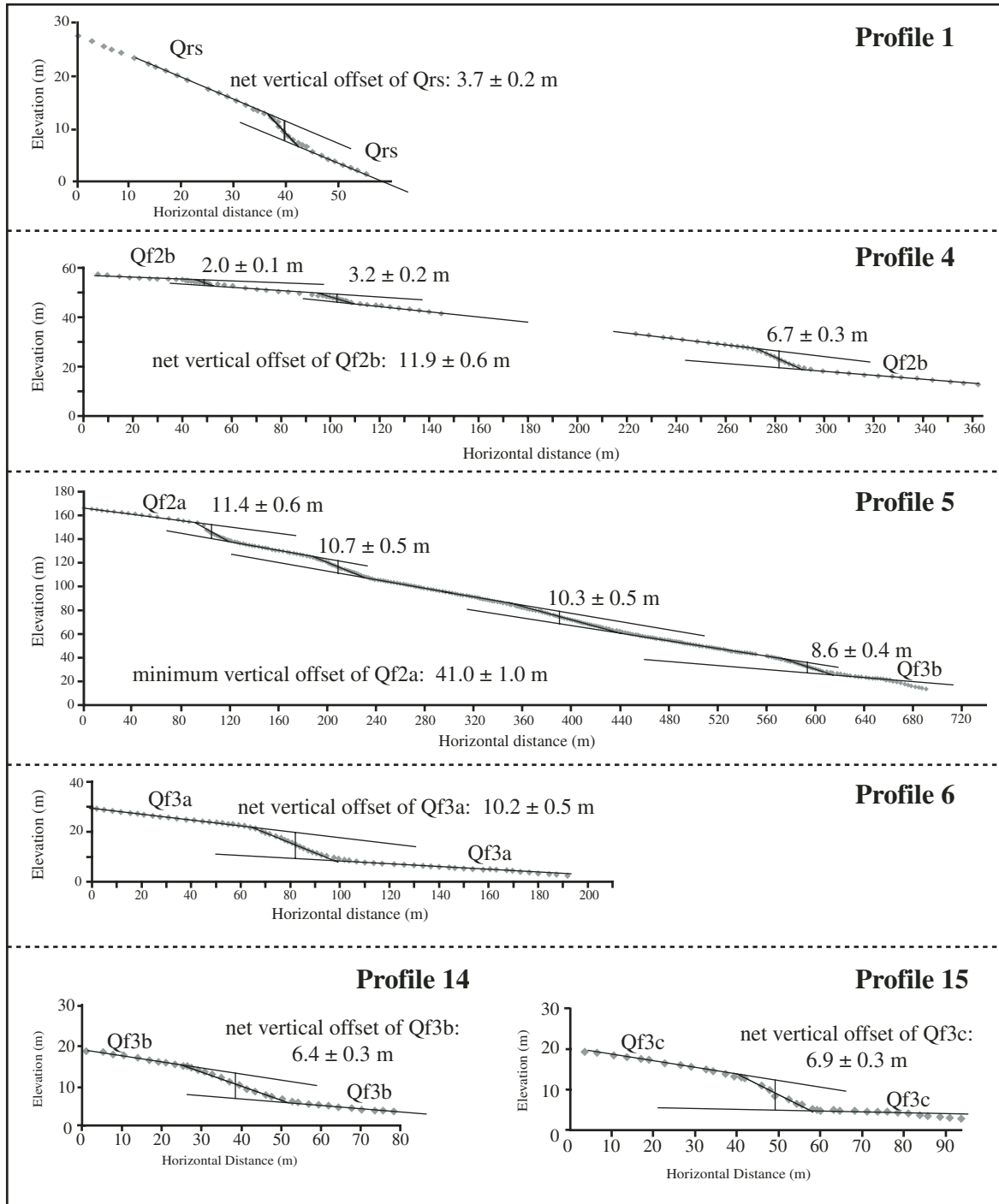


Figure 9. Selected topographic profiles across alluvial fan surfaces and calculated vertical offsets. See Figures 3 and 5 for locations of profiles, and Figure 7 for definition of a fault scarp.

TABLE 3. MEASURED VERTICAL OFFSETS FROM PROFILES

| Profile | Footwall | | Surface | Farfield slope | Hanging wall | | Surface | Farfield slope | Fault-scarp slope [‡] | Vertical offset [§] (m) |
|------------------|-----------------------|------------------------|---------|----------------|-----------------------|------------------------|---------|----------------|--------------------------------|----------------------------------|
| | Latitude [†] | Longitude [†] | | | Latitude [†] | Longitude [†] | | | | |
| P22 | 36°33'41.88494"N | 118°10'37.85137"W | Bedrock | 9° | 36°33'52.43491"N | 118°10'20.74796"W | Qf3b | 4° | 51° | 130.0 ± 6.5 |
| P11 | 36°41'37.66708"N | 118°14'46.58583"W | Qf1 | 10° | 36°41'40.65751"N | 118°14'44.00062"W | Qf3b | 8° | 22° | 24.3 ± 1.2 |
| P12 | 36°40'34.88331"N | 118°14'32.92758"W | Qf1 | 16° | 36°40'38.59162"N | 118°14'24.22065"W | Qf2b | 7° | 25° | 40.8 ± 2.0 |
| P13 | 36°40'25.57094"N | 118°13'56.50982"W | Qf1 | 5° | 36°40'28.91584"N | 118°13'45.84125"W | Qf1 | 7° | 14° | 12.5 ± 0.6 |
| P8 | 36°44'24.58454"N | 118°16'06.10728"W | Qf1 | 7° | 36°44'35.94515"N | 118°15'51.61858"W | Qf3b | 2° | 18° | 36.2 ± 1.8 |
| P7 | 36°42'36.99164"N | 118°15'50.50001"W | Qf2a | 10° | 36°42'43.87871"N | 118°15'31.81631"W | Qf2a | 9° | 17° | 24.6 ± 1.2 |
| P9 | 36°42'30.19230"N | 118°15'45.33960"W | Qf2a | 6° | 36°42'39.32798"N | 118°15'22.22600"W | Qf2a | 3° | 11° | 14.7 ± 0.7 |
| P2 [#] | 36°46'01.43271"N | 118°17'10.41829"W | Qf2a | 8° | 36°45'59.88147"N | 118°16'50.36334"W | Qf2b | 5° | 14° | 26.8 ± 1.3 |
| P5 [#] | 36°43'26.10181"N | 118°16'36.72235"W | Qf2a | 10° | 36°43'29.53096"N | 118°16'08.90832"W | Qf3b | 9° | 18° | 41.0 ± 2.1 |
| P17 | 36°34'09.35298"N | 118°10'57.65334"W | Qf2a | 11° | 36°34'24.11814"N | 118°10'08.61804"W | Qf2a | 9° | 16° | 36.1 ± 1.8 |
| P3 | 36°43'44.39258"N | 118°16.34.88166"W | Qf2b | 9° | 36°44'35.94515"N | 118°15'51.61858"W | Qf2b | 4° | 18° | 21.9 ± 1.1 |
| P4 | 36°43'46.88502"N | 118°16'34.23807"W | Qf2b | 4° | 36°43'53.45056"N | 118°16'23.91553"W | Qf2b | 4° | 24° | 11.9 ± 0.6 |
| P18 | 36°33'23.04777"N | 118°10'16.00147"W | Qf2b | 9° | 36°33'25.40037"N | 118°10'03.61028"W | Qf2b | 9° | 16° | 8.7 ± 0.4 |
| P16 | 36°46'01.39507"N | 118°17'09.95666"W | Qf2b | 9° | 36°45'59.88147"N | 118°16'50.36334"W | Qf2b | 7° | 17° | 23.9 ± 1.2 |
| P6 | 36°43'10.85918"N | 118°16'05.62269"W | Qf3a | 6° | 36°43'12.40892"N | 118°16'03.19851"W | Qf3a | 3° | 21° | 10.2 ± 0.5 |
| P20 | 36°31'58.55119"N | 118°08'10.66049"W | Qf3a | 9° | 36°31'57.74456"N | 118°07'59.51543"W | Qf3a | 7° | 22° | 6.4 ± 0.3 |
| P10 | 36°41'40.62442"N | 118°14'46.04716"W | Qf3b | 10° | 36°41'41.05906"N | 118°14'44.55919"W | Qf3b | 3° | 18° | 5.0 ± 0.3 |
| P19 | 36°32'01.00655"N | 118°08'11.69983"W | Qf3b | 6° | 36°32'01.00655"N | 118°08'08.74409"W | Qf3b | 6° | 27° | 5.9 ± 0.3 |
| P14 | 36°39'29.45048"N | 118°13'51.91144"W | Qf3b | 10° | 36°39'31.00879"N | 118°13'49.57784"W | Qf3b | 2° | 22° | 6.4 ± 0.3 |
| P21 | 36°32'00.97444"N | 118°08'11.44998"W | Qf3b | 12° | 36°32'01.61168"N | 118°08'08.19008"W | Qf3b | 8° | 33° | 5.4 ± 0.3 |
| P15 | 36°39'26.70070"N | 118°13'47.78341"W | Qf3c | 9° | 36°39'27.12859"N | 118°13'46.20921"W | Qf3c | 2° | 23° | 6.9 ± 0.3 |
| P1 ^{††} | 36°47'54.25441"N | 118°18'33.22265"W | Qrs | 25° | 36°47'54.19420"N | 118°18'31.01171"W | Qrs | 24° | 49° | 3.7 ± 0.2 |

[†]Latitude and longitude values listed are for each end of the topographic profile measured.

[‡]Fault-scarp slope angles are averages for those surfaces with multiple fault scarps.

[§]Vertical offset measurements are minimum vertical offsets for those scarps with younger surfaces in the hanging-wall surface.

[#]Fault-scarp profiles excluded in the calculation of the weighted mean vertical offset.

^{††}Vertical offset measured just south of the rockslide, owing to the undulating surface of the rockslide. See text for explanation.

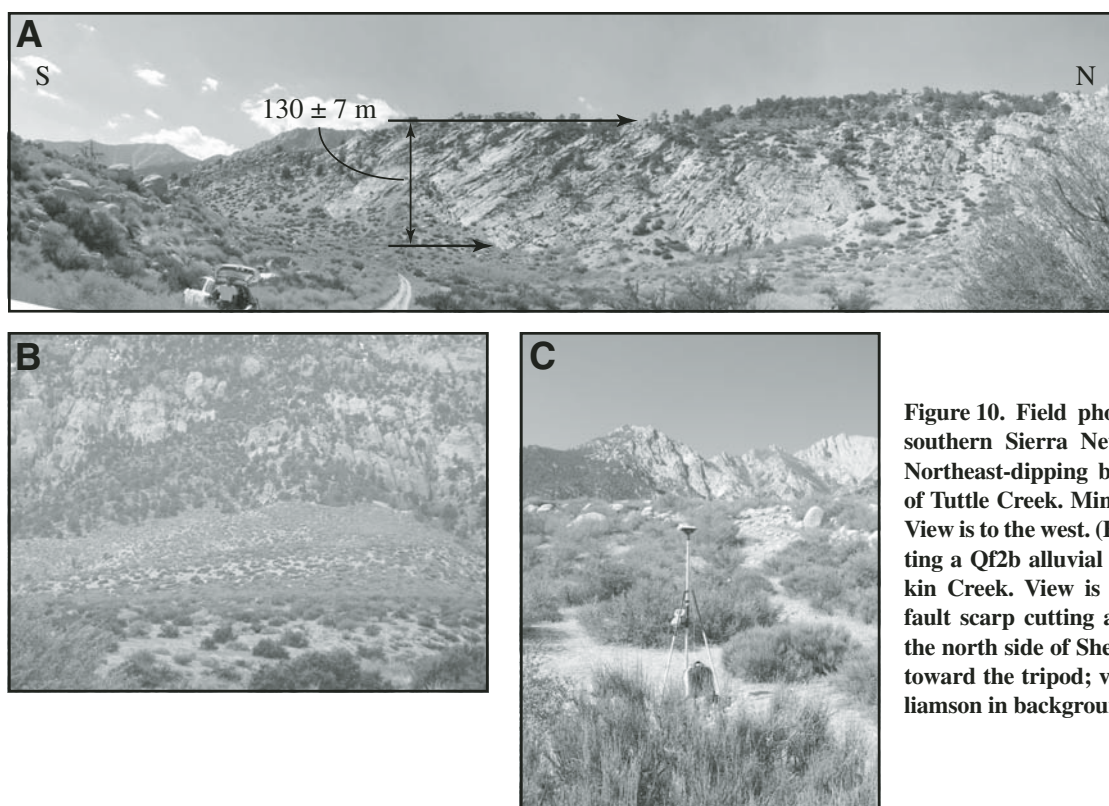


Figure 10. Field photos of fault scarps along the southern Sierra Nevada frontal fault scarp. (A) Northeast-dipping bedrock fault scarp just north of Tuttle Creek. Minimum vertical offset is shown. View is to the west. (B) East-dipping fault scarp cutting a Qf2b alluvial fan surface just south of Lubkin Creek. View is to the west. (C) East-dipping fault scarp cutting a Qf3a alluvial fan surface on the north side of Shepherd Creek. Fault scarp dips toward the tripod; view is to the west. Mount Williamson in background.

TABLE 4. SUMMARY OF SURFACE AGES, VERTICAL OFFSETS, AND SLIP RATES

| Surface | Age [†] ± error (ka) | Vertical offset of dated surface (m) | Weighted mean vertical offset (m) [‡] | Maximum vertical offset (m) [§] | Vertical slip rate (mm/yr) [#] | Horizontal slip rate (mm/yr) ^{††} |
|---------|-------------------------------|--------------------------------------|--|--|---|--|
| Qf1 | 123.7 ± 16.6 | 24.3 ± 1.2 ^{‡‡} | — | 40.8 ± 2.0 ^{‡‡} | 0.2–0.3 ± 0.1 ^{§§} | 0.1–0.2 ± 0.1 ^{§§} |
| Qf2a | Qf1>Qf2a>Qf2b | — | 21.8 ± 0.5 | 41.0 ± 2.1 | 0.7 ± 0.1>vsr>0.2 ± 0.1 | 0.4 ± 0.1>hsr>0.1 ± 0.1 |
| Qf2b | 60.9 ± 6.6 | 11.9 ± 0.6 | 11.3 ± 0.3 | 23.9 ± 1.2 | 0.2–0.4 ± 0.1 | 0.1–0.2 ± 0.1 |
| Qf3a | 25.8 ± 7.5 | 10.2 ± 0.5 | 7.4 ± 0.3 | 10.2 ± 0.5 | 0.3–0.4 ± 0.1 | 0.2 ± 0.1 |
| Qf3b | Qf3a>Qf3b>Qf3c | — | 5.7 ± 0.2 | 6.4 ± 0.3 | 1.5 ± 0.4>vsr>0.3 ± 0.1 | 0.9 ± 0.4>hsr>0.2 ± 0.1 |
| Qf3c | 4.4 ± 1.1 | — | — | 6.9 ± 0.3 | 1.6 ± 0.4 | 0.9 ± 0.4 |

Note: vsr—vertical slip rate; hsr—horizontal slip rate.

[†]Age estimates are calculated using a boulder surface erosion rate of 0.3 cm/k.y.

[‡]Weighted mean vertical offset for fault scarps with the same surface in the hanging wall and the footwall (see Table 3).

[§]Maximum measured surface offset (see Table 3).

[#]Vertical slip rates are calculated for the time period since the surface was abandoned and show a range of rates that incorporate measured offset of dated surface, maximum, and weighted mean values.

^{††}Slip rates are calculated assuming a 60° fault dip.

^{‡‡}Vertical offset is a minimum for fault scarps with younger hanging-wall surfaces.

^{§§}Slip-rate estimates are a minimum.

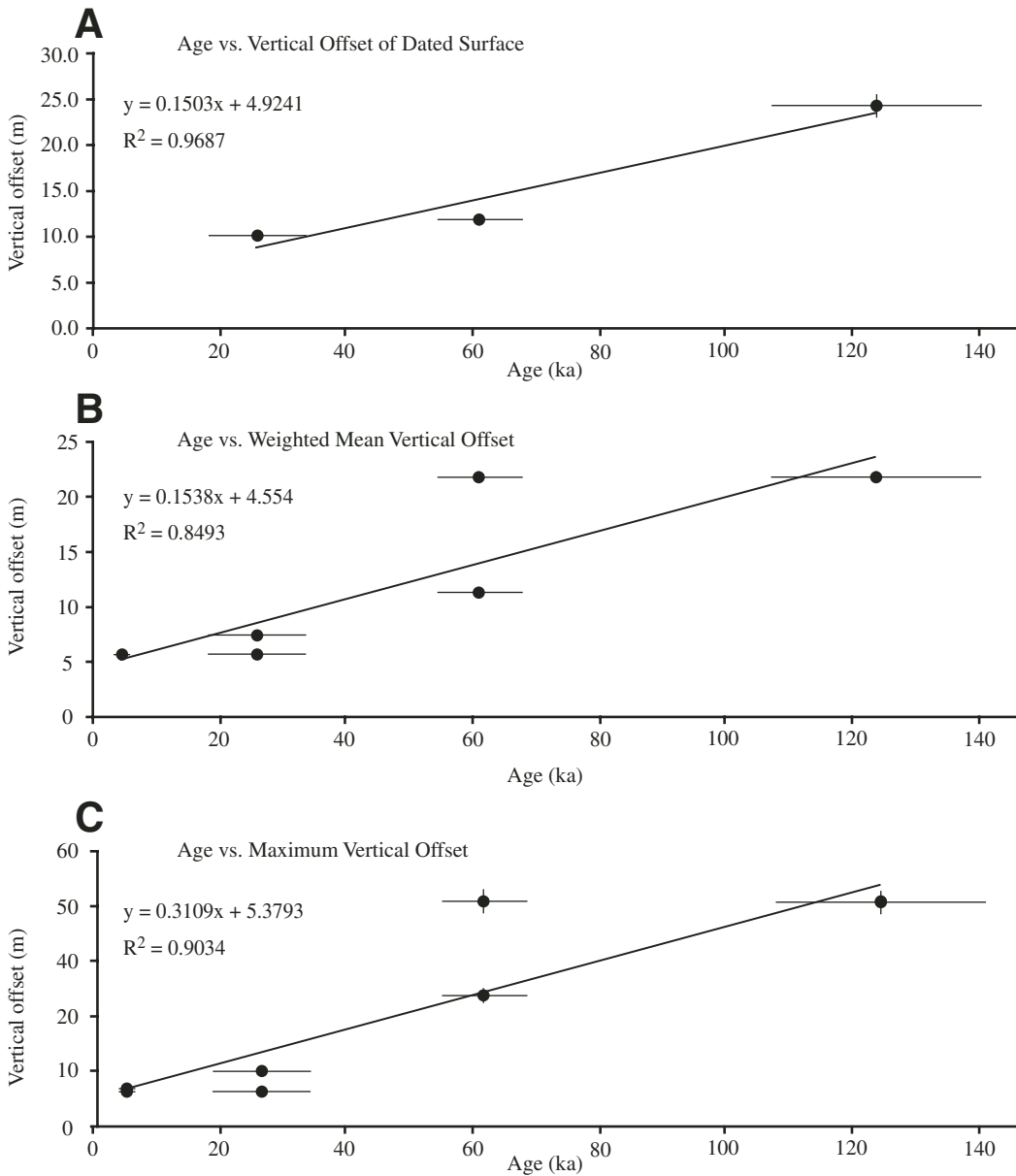


Figure 11. Surface age vs. vertical offset plots for (A) dated surface vertical offsets, (B) weighted mean vertical offsets, and (C) maximum vertical offsets (see Table 4). Linear regressions through these data yield average late Pleistocene to Holocene vertical slip rates of 0.2–0.3 mm/yr across the Sierra Nevada frontal fault zone. Errors indicated by lines through data points; data points commonly are larger than error associated with vertical offset values.

TABLE 5. SUMMARY OF VERTICAL SLIP RATES FOR THE SIERRA NEVADA REGION

| Fault | Slip rate (mm/yr) | Reference |
|-----------------------------|------------------------|---|
| Lone Pine fault | 0.5 ± 0.2 | Lubetkin and Clark (1988); Beanland and Clark (1994) |
| Fish Springs fault | 0.2 ± 0.1 | Martel et al. (1987); Zehfuss et al. (2001) |
| Northern SNFFZ [†] | 0.4 ± 0.1 to 0.9 ± 0.2 | Kent et al. (2005) |
| Central SNFFZ | 0.4 ± 0.1 to 0.9 ± 0.2 | Berry (1989) |
| Southern SNFFZ [‡] | >1 | Clark and Gillespie (1993) |
| Southern SNFFZ [§] | 0.2 ± 0.1 to 0.4 ± 0.1 | This study |

Note: SNFFZ—Sierra Nevada frontal fault zone.
[†]Slip-rate determination at the latitude of Lake Tahoe.
[‡]Slip-rate determination at the latitude of Round Valley.
[§]Slip-rate determination at the latitude of the Alabama Hills.

a discrepancy may not exist, because Sierran-derived sandstones, gravels, and boulders observed in ca. 8 Ma basin deposits along the southeasternmost Sierra Nevada imply tectonic uplift at this time (Loomis and Burbank, 1988).

Our vertical slip-rate estimates are also the same as those for several range-bounding normal faults within the Basin and Range Province to the east (e.g., Wesnousky et al., 2005; U.S. Geological Survey, 2004; Friedrich et al., 2004; Hayman et al., 2003; Machette et al., 1992). Documented Quaternary vertical slip rates along the Wasatch fault zone, which defines the eastern boundary of the Basin and Range Province, are 0.3–0.6 mm/yr, comparable to our vertical slip rates (Machette et al., 1992; McCaplin and Nishenko, 1996; Davis et al., 2003). In the central region of the Basin and Range Province, long-term geologic slip rates of ~0.3 mm/yr have been documented along the Crescent Valley fault (Friedrich et al., 2004), and 0.2 ± 0.1–1.0 ± 0.2 mm/yr have been documented along the Dixie Valley fault (Caskey et al., 1996). To the west, along the western boundary of the Basin and Range Province, the Black Mountain fault zone in Death Valley yields vertical slip rates of ~0.5 ± 0.1 mm/yr (Hayman et al., 2003). Long-term geologic vertical slip-rate estimates across range-bounding normal faults within the Basin and Range Province are ~0.2–0.4 ± 0.1 mm/yr (Bennett et al., 2003; Friedrich et al., 2003), similar to our calculated average late Pleistocene to Holocene slip rates across the Sierra Nevada frontal fault zone.

If we assume that this fault zone and the Lone Pine fault dip 60° and 75° (Beanland and Clark, 1994), respectively, then summing their late Pleistocene horizontal extension rates yields an estimated horizontal extension rate of 0.3 ± 0.1 mm/yr across Owens Valley at the latitude of Lone Pine. Shallower dipping faults will result in a higher rate of extension, whereas more steeply dipping faults will result in a lower rate of extension.

The closely spaced Sierra Nevada frontal fault zone, Lone Pine fault, and Owens Valley fault accommodate both extension and dextral shear along the western boundary of the Basin and Range Province—Eastern California Shear Zone. The mix of normal faulting and strike-slip faulting in this region, and the northern continuation of the Eastern California Shear Zone and the Walker Lane Belt, have been interpreted as either spatially and/or temporally varying regional stresses (e.g., Wright, 1976; Stewart, 1988; Zoback and Zoback, 1989; Bellier and Zoback, 1995; Monastero et al., 2002) or fault-slip partitioning within a single regional stress field (e.g., Wesnousky and Jones, 1994; Oldow, 1992). Both hypotheses have been proposed for the coexistence of the high-angle, dip-slip Sierra Nevada frontal fault zone and the vertical, dextral-slip Owens Valley fault (Zoback, 1989; Wesnousky and Jones, 1994; Bellier and Zoback, 1995).

Based on fault-slip azimuth data, Zoback and Zoback (1989) and Bellier and Zoback (1995) postulated that the stress regime along this section of the Sierra Nevada underwent a recent (<100,000 yr, but >10,000 yr) permanent change from normal-slip-dominated to strike-slip-dominated stress regimes. Because of the absence of geochronologic data, Bellier and Zoback (1995) noted that rather than a single change in stress regime, there could have been cyclic fluctuations. Critical to this interpretation were observations of crosscutting fault striations, commonly assumed to have formed as the result of multiple slip events at different times, along the northern part of the Owens Valley fault (Bellier and Zoback, 1995). However, crosscutting fault striations have been observed along fault planes exposed during a number of earthquakes, including the 1992 Landers, the 1969 Pariahuanca, Peru (Philip and Megard, 1977), and the 1980 El Asnam, Algeria (Philip and Meghraoui, 1983), earthquakes. Furthermore, dynamic modeling of fault rupture at low stress by Spudich et al.

(1998) showed that curved or crosscutting fault striations can form during an earthquake. Thus, field observations and modeling provide an alternative interpretation to the commonly held view that crosscutting striations are the result of different slip events at different times. Finally, the pre-1872 rupture along the Owens Valley fault (3.3 ± 0.3–3.8 ± 0.3 ka) (Lee et al., 2001) and the last earthquake along the Sierra Nevada frontal fault zone (≤4.1 ± 1.1 ka; this study) occurred at most 2000 yr apart, implying a rapid change in stress regime if this hypothesis is valid.

In the second hypothesis, this region is characterized by a single stress field, and motion of the southern Sierra Nevada is partitioned (Wesnousky and Jones, 1994) in this case into three components—dominant dextral slip along the Owens Valley fault, intermediate oblique slip on the Lone Pine fault, and subordinate normal slip along the Sierra Nevada frontal fault zone. Using stress transformation laws (Jones and Wesnousky, 1992) and a simple physical model, whereby one principal stress is vertical and slip vectors on a fault parallel the shear stress resolved on that fault plane, oblique extension is partitioned onto a dipping fault and a parallel, vertical, strike-slip fault (Wesnousky and Jones, 1994). Jones and Wesnousky (1992) derive an expression for the ratio of shear resistance *R* between the strike-slip fault (τ_s) and dipping fault (τ_d):

$$R = \tau_s / \tau_d = \sin\psi / [\sin\Delta(1 + \cos^2\psi \tan^2\Delta)^{1/2}], \quad (1)$$

where Δ = dip of fault plane and ψ = azimuth of slip on the dipping fault. This equation indicates that when fault slip is partitioned, oblique extension is controlled by fault dip Δ and shear resistance ratio *R*, and not slip azimuth. Furthermore, the relative strengths along faults across which slip has been partitioned can be determined by knowing fault dip and slip azimuth. Fault slip and dip azimuth data from the Sierra Nevada frontal fault zone, Lone Pine fault, and Owens Valley fault show that the Sierra Nevada frontal fault zone is considerably stronger (approximately two orders of magnitude) than either the Lone Pine or Owens Valley fault (Table 6; Fig. 12). We conclude that the available data

TABLE 6. SUMMARY OF FAULT DIP AND SLIP AZIMUTH

| Faults | Average strike | Dip angle, Δ (°) | Slip azimuth, ψ (°) |
|--------------------|----------------|-------------------------|--------------------------|
| Owens Valley fault | 340° | 85 ± 10 | 80–90 |
| Lone Pine fault | 340° | 75 ± 10 | 70–80 |
| SNFFZ | 340° | 60 ± 10 | 0–2 |

Note: SNFFZ—Sierra Nevada frontal fault zone.

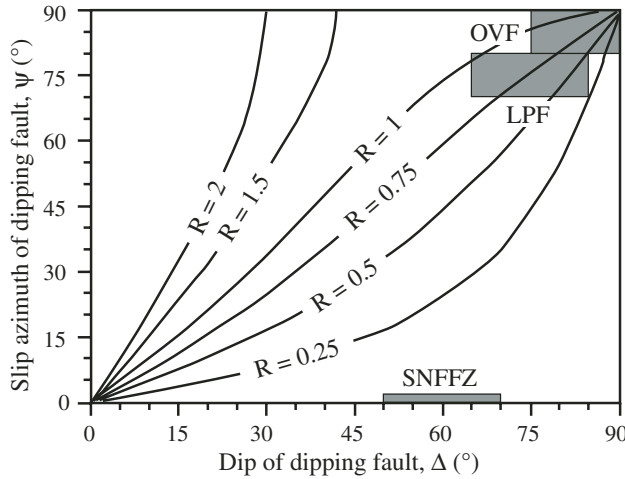


Figure 12. Contours of constant R values (see equation 1 in text) on a plot of fault-dip angle Δ vs. slip azimuth ψ . Given observed values of Δ and ψ on the Owens Valley fault, Lone Pine fault, and Sierra Nevada frontal fault zone (Table 6), R for the Owens Valley and Lone Pine faults is approximately two orders of magnitude greater than that for the Sierra Nevada frontal fault zone. OVF—Owens Valley fault; LPF—Lone Pine fault; SNFFZ—Sierra Nevada frontal fault zone.

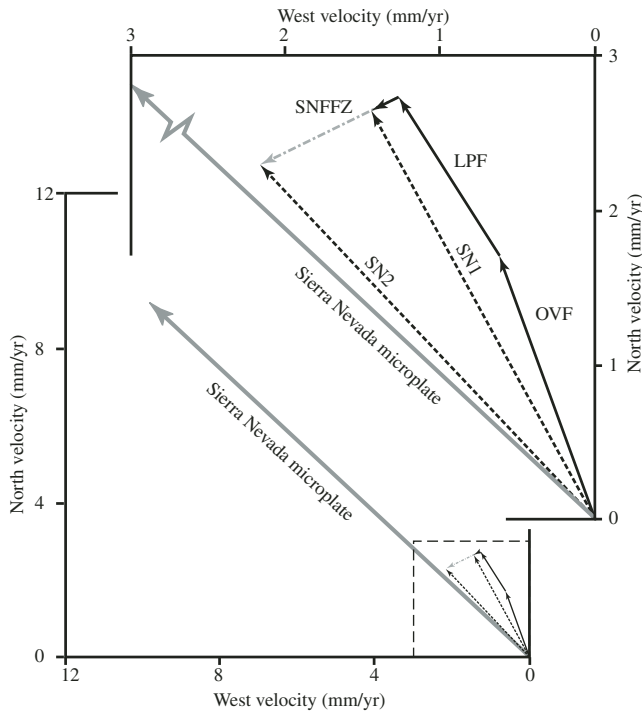


Figure 13. Velocity vector diagram showing predicted motion of the Sierra Nevada (dashed lines) along the Owens Valley, Lone Pine, and Sierra Nevada frontal faults with respect to a block east of the Owens Valley fault. Vector SN1 shows predicted motion of the Sierra Nevada, assuming that late Pleistocene slip rates along the Sierra Nevada frontal fault zone have remained constant into the Holocene, whereas vector SN2 shows predicted motion of the Sierra Nevada, assuming that slip rates increased along the Sierra Nevada frontal fault zone during the Holocene. Azimuth of the Sierra Nevada microplate with respect to stable North America shown as a heavy gray arrow (Dixon et al., 2000). This diagram uses a dextral slip-rate estimate for the Owens Valley fault of 1.8 ± 0.3 mm/yr (Lee et al., 2001). SNFFZ—Sierra Nevada frontal fault zone; LPF—Lone Pine fault; OVF—Owens Valley fault; SN—Sierra Nevada. See text for discussion.

on crosscutting fault striations, timing of earthquakes, and relative fault strengths suggest that transtensional motion of the Sierra Nevada block is best explained by fault-slip partitioning within a single regional stress field.

The Sierra Nevada frontal fault zone, Lone Pine fault, and Owens Valley fault (Fig. 1) form a triad normal-oblique, strike-slip fault system with estimated late Pleistocene to Holocene horizontal extension, oblique, and dextral slip rates of 0.1–0.2 mm/yr (azimuth of 64°), 1.2 ± 0.6 mm/yr (azimuth of 328°), and 1.8 ± 0.3 mm/yr (Lee et al., 2001; azimuth of 340°), respectively. These subparallel faults strike clockwise with respect to the $\sim 313^\circ$ -trending vector that defines motion of the Sierra Nevada microplate relative to stable North America (Dixon et al., 2000), yet only the Lone Pine fault exhibits oblique slip (Lubetkin and Clark, 1988; Beanland and Clark, 1994). These relations imply that motion of the southern Sierra Nevada is partitioned into three components—dominant dextral slip along the Owens Valley fault, intermediate oblique slip on the Lone Pine fault, and subordinate normal slip along the Sierra Nevada frontal fault zone. If we assume that late Pleistocene slip rates along the Sierra Nevada frontal fault zone have remained constant into the Holocene, a velocity vector diagram shows that motion of the Sierra Nevada with respect to a fixed block east of the Owens Valley fault is at a rate of ~ 3.0 mm/yr toward an azimuth of $\sim 331^\circ$ (Fig. 13). The summed Sierra Nevada vector is clockwise with respect to motion of the Sierra Nevada microplate relative to stable North America. This difference can be explained by extension across the Basin and Range Province between the Owens Valley fault and stable North America (e.g., Wernousky et al., 2005; U.S. Geological Survey, 2004; Friedrich et al., 2004; Thatcher et al., 1999; Wernicke et al., 2000). If, on the other hand, our higher Holocene slip rates reflect an increase in strain rate along the Sierra Nevada frontal fault zone, then motion of the Sierra Nevada has a rate of ~ 3.2 mm/yr toward an azimuth of $\sim 317^\circ$, nearly parallel to the Sierra Nevada block motion (Fig. 13). Note that if we use Bacon et al.’s (2002) dextral slip-rate estimate of 0.8 mm/yr along the Owens Valley fault, it yields a predicted motion of the Sierra Nevada that ranges from a rate of ~ 2.0 mm/yr toward an azimuth of 327° to a rate of ~ 2.3 mm/yr toward an azimuth of 306° . The distribution of fault slip along the eastern escarpment of the Sierra Nevada shows that dextral slip dominates, consistent with measured GPS velocities across the western margin of the Basin and Range Province (e.g., Thatcher et al., 1999; Wernicke et al., 2000).

CONCLUSIONS

New geologic mapping and ^{10}Be alluvial-fan-surface abandonment ages along the southern Sierra Nevada frontal fault zone yield numerical ages for several alluvial fan surfaces that range from ca. 124 to 4 ka and geomorphic evidence that slip along faults that cut these surfaces is normal dip slip. Vertical slip across fault scarps that cut alluvial fan surfaces ranges from ~41 to 4 m. Combining these data yields an average late Pleistocene to Holocene vertical slip rate of 0.2–0.3 mm/yr, which is similar to late Pleistocene to Holocene slip rates documented along bounding normal faults of the Basin and Range Province. The motion of the Sierra Nevada block is partitioned onto three subparallel, closely spaced faults along its southeastern flank: subordinate normal slip along the Sierra Nevada frontal fault zone, intermediate oblique slip along the Lone Pine fault, and dominant dextral slip along the Owens Valley fault. Distribution of slip rates among these three faults demonstrates that dextral slip has dominated since at least the late Pleistocene, consistent with the dextrally dominated present-day transtensional strain accumulation observed across the western margin of the Eastern California Shear Zone and the Basin and Range Province.

ACKNOWLEDGMENTS

Comments by John Wakabayashi and Paul Zehfuss on a shorter version of this manuscript and discussions with Tim Dixon were valuable. Informative reviews by Chris Henry, Craig Jones, and John Wakabayashi greatly improved this manuscript. Thanks to Jeff Schroeder for help with field mapping, and Andrew Minor, Carrie Thau, John Thau, Luke Swan, Jason Dorsch, and Marie-Luce Chevalier for assistance with GPS surveying and processing. This research was supported by U.S. National Science Foundation grants EAR-0207365 and EAR-0207245 and grants from Sigma Xi and the White Mountain Research Station awarded to K. Le, and was performed under the auspices of the U.S. Department of Energy by the University of California and the Lawrence Livermore National Laboratory under contract no. W-7405-Eng-48.

REFERENCES CITED

Argus, D.F., and Gordon, R.G., 1991, Current Sierra Nevada–North America motion from very long baseline interferometry; implications for the kinematics of the Western United States: *Geology*, v. 19, p. 1085–1088, doi: 10.1130/0091-7613(1991)019<1085:CSNNAM>2.3.CO;2.

Arrowsmith, J.R., Rhodes, D.D., and Pollard, D.D., 1998, Morphologic dating of scarps formed by repeated slip events along the San Andreas fault, Carrizo Plain, California: *Journal of Geophysical Research*, v. 103, p. 10,141–10,160, doi: 10.1029/98JB00505.

Bacon, S.N., Pezzopane, S.K., and Burke, R.M., 2002, Paleoseismology on the Owens Valley fault and Holocene stratigraphy of pluvial Owens Lake near Lone Pine, eastern California: *Geological Society of America Abstracts with Programs*, v. 34, no. 6, p. 27.

Bateman, P.C., and Eaton, J.P., 1967, Sierra Nevada Batholith: *Science*, v. 158, p. 1407–1417.

Bateman, P.C., and Wahrhaftig, C., 1966, Geology of the Sierra Nevada, in Bailey, E.H., ed., *Geology of Northern California*: California Division of Mines and Geology Bulletin 190, p. 107–172.

Beanland, S., and Clark, M.M., 1994, The Owens Valley fault zone, eastern California, and surface faulting associated with the 1872 earthquake: *U.S. Geological Survey Bulletin* 1982, 29 p.

Bellier, O., and Zoback, M.L., 1995, Recent state of stress change in the Walker Lane zone, western Basin and Range Province, United States: *Tectonics*, v. 14, p. 564–593, doi: 10.1029/94TC00596.

Bennett, R., Wernicke, B., Neimi, N.A., Friedrich, A.M., and Davis, J.L., 2003, Contemporary strain rates in the northern Basin and Range Province from GPS data: *Tectonics*, v. 22, 1008, doi: 10.1029/2001TC001355.

Berry, M.E., 1989, Soil-geomorphic analysis of late-Pleistocene glacial sequences, the McGee, Pine, and Bishop Creek drainages, east-central Sierra Nevada, California [Ph.D. thesis]: Palo Alto, California, Stanford University, 235 p.

Bierman, P.R., Gillespie, A.R., and Caffee, M.W., 1995, Cosmogenic ages for recurrence intervals and debris flow fan deposition, Owens Valley, California: *Science*, v. 270, p. 447–450.

Blair, T.C., 2001, Outburst flood sedimentation on the proglacial Tuttle Canyon alluvial fan, Owens Valley, California, U.S.A.: *Journal of Sedimentary Research*, v. 71, p. 657–679.

Caskey, S.J., Wesnousky, S.G., Zhang, P., and Slemmons, D.B., 1996, Surface faulting of the 1954 Fairview Peak (Ms 7.2) and Dixie Valley (Ms 6.8) earthquakes, central Nevada: *Bulletin of the Seismological Society of America*, v. 86, p. 761–787.

Christensen, M.N., 1966, Late Cenozoic crustal movements in the Sierra Nevada of California: *Geological Society of America Bulletin*, v. 77, p. 163–182.

Clark, D., 1972, Range-front faulting: Cause of anomalous relations among moraines of the eastern slope of the Sierra Nevada, California: *Geological Society of America Cordilleran Section Abstracts and Sections*, p. 137.

Clark, M.M., and Gillespie, A.R., 1993, Variations in late Quaternary behavior along and among range-front faults of the Sierra Nevada, California: *Geological Society of America Abstracts with Programs*, v. 25, no. 5, p. 21.

Davis, J.L., Bennett, R.A., and Wernicke, B.P., 2003, Assessment of GPS velocity accuracy for the Basin and Range Geodetic Network (BARGEN): *Journal of Geophysical Research Letters*, v. 31, no. 7, p. 1411.

Dixon, T.H., Miller, M., Farina, F., Wang, H., and Johnson, D., 2000, Present-day motion of the Sierra Nevada block, and some tectonic implications for the Basin and Range Province: *North American Cordillera: Tectonics*, v. 19, p. 1–24, doi: 10.1029/1998TC001088.

Flesch, L.M., Holt, W.E., Haines, A.J., and Shen-Tu, B., 2000, Dynamic of the Pacific–North American plate boundary zone in the western United States: *Science*, v. 287, p. 834–836, doi: 10.1126/science.287.5454.834.

Friedrich, A.M., Wernicke, B.P., Niemi, N.A., Bennett, R.A., and Davis, J.L., 2003, Comparison of geodetic and geologic data from the Wasatch region, Utah, and implications for the spectral character of the Earth deformation at periods of 10 years to 10 million years: *Journal of Geophysical Research*, v. 108, no. B4, 2199, doi: 10.1029/2001JB000682.

Friedrich, A.M., Lee, J., Wernicke, B.P., and Sieh, K., 2004, Geologic context of geodetic data across the Basin and Range normal fault, Crescent Valley, Nevada: *Tectonics*, v. 23, TC2015, doi: 10.1029/2003TC001528.

Gillespie, A.R., 1982, Quaternary glaciation and tectonism in the southern Sierra Nevada, Inyo County, California [Ph.D. thesis]: Pasadena, California Institute of Technology, 736 p.

Gosse, J.C., and Phillips, F.M., 2001, Terrestrial in-situ cosmogenic nuclides: Theory and applications: *Quaternary Science Reviews*, v. 20, p. 1475–1560, doi: 10.1016/S0277-3791(00)00171-2.

Hammond, W.C., and Thatcher, W., 2004, Contemporary tectonic deformation of the Basin and Range province, western United States: 10 years of observation with the Global Positioning System: *Journal of Geophysical Research*, v. 109, B08403, doi: 10.1029/2003JB002746.

Hanks, T.C., Bucknam, R.C., Lajoie, K.R., and Wallace, R.E., 1984, Modification of wave-cut and fault controlled landforms: *Journal of Geophysical Research*, v. 89, p. 5771–5790.

Hayman, N.W., Knott, J.R., Cowen, D.S., Nemster, E., and Sarna-Wojcicki, A.M., 2003, Quaternary low-angle slip on detachment faults in Death Valley, California: *Geology*, v. 31, p. 343, doi: 10.1130/0091-7613(2003)031<0343:QLASOD>2.0.CO;2.

Jones, C.H., and Wesnousky, S.G., 1992, Variations in strength and slip rate along the San Andreas Fault system: *Science*, v. 256, p. 83–86.

Jones, C.H., Farmer, G.L., and Unruh, J., 2004, Tectonics of Pliocene removal of lithosphere of the Sierra Nevada, California: *Geological Society of America Bulletin*, v. 116, p. 1408–1422, doi: 10.1130/B25397.1.

Kent, G.M., Babcock, J.M., Driscoll, N.W., Harding, A.J., Dinger, J.A., Seitz, G.G., Gardner, J.V., Mayer, L.A., Goldman, C.R., Heyvaert, A.C., Richards, R.C., Karlin, R., Morgan, C.W., Gayes, P.T., and Owen, L.A., 2005, 60 k.y. record of extension across the western boundary of the Basin and Range province: Estimate of slip rates from offset shoreline terraces and a catastrophic slide beneath Lake Tahoe: *Geology*, v. 33, p. 365–368, doi: 10.1130/G21230.1.

Kohl, C.P., and Nishiizumi, K., 1992, Chemical isolation of quartz for measurement of in-situ-produced cosmogenic nuclides: *Geochimica et Cosmochimica Acta*, v. 56, p. 3583–3587, doi: 10.1016/0016-7037(92)90401-4.

Lal, D., 1991, Cosmic ray labeling of erosion surfaces: In-situ nuclide production rates and erosion models: *Earth and Planetary Science Letters*, v. 104, p. 424–439, doi: 10.1016/0012-821X(91)90220-C.

Lee, J., Spencer, J., and Owen, L., 2001, Holocene slip rates along the Owens Valley fault, California: Implications for the recent evolution of the Eastern California Shear Zone: *Geology*, v. 29, p. 819–822, doi: 10.1130/0091-7613(2001)029<0819:HSRATO>2.0.CO;2.

Lindgren, W., 1911, The Tertiary gravels of the Sierra Nevada, California: *U.S. Geological Survey Professional Paper* 73, 226 p.

Loomis, D.P., and Burbank, D.W., 1988, The stratigraphic evolution of the El Paso basin, southern California: Implications for the Miocene development of the Garlock fault and uplift of the Sierra Nevada: *Geological Society of America Bulletin*, v. 100, p. 12–28, doi: 10.1130/0016-7606(1988)100<0012:TSEOTE>2.3.CO;2.

Lubetkin, L., and Clark, M., 1988, Late Quaternary activity on the Lone Pine fault, eastern California: *Geological Society of America Bulletin*, v. 100, p. 755–766, doi: 10.1130/0016-7606(1988)100<0755:LQAATL>2.3.CO;2.

Machette, M.N., Personius, S.F., Nelson, A.R., Bucknam, R.C., and Hancock, P.L., 1992, The Wasatch fault zone, U.S.A.: *Annales Tectonicae*, v. 6, p. 5–39.

Martel, S.J., Harrison, T.M., and Gillespie, A.R., 1987, Late Quaternary vertical displacement rate across the Fish Springs fault, Owens Valley fault zone, California: *Quaternary Research*, v. 27, p. 113–129, doi: 10.1016/0033-5894(87)90071-8.

McCalpin, J.P., 1996, *Paleoseismology*: New York, Academic Press, v. 62, p. 91–135.

McCalpin, J.P., and Nishenko, S.P., 1996, Holocene paleoseismicity, temporal clustering, and probabilities of future large ($M > 7$) earthquakes on the Wasatch fault zone, Utah: *Journal of Geophysical Research*, v. 101, p. 6233–6253.

Monastero, F.C., Walker, J.D., Katzenstein, A.M., and Sabin, A.E., 2002, Neogene evolution of the Indian Wells Valley, east-central California, in Glazner, A.F., et al., eds., *Geologic evolution of the Mojave Desert and southwestern Basin and Range*: *Geological Society of America Memoir* 195, p. 199–228.

Muzikar, P., Elmore, D., and Granger, D.E., 2003, Accelerator mass spectrometry in geologic research: *Geological Society of America Bulletin*, v. 115, p. 643–654, doi: 10.1130/0016-7606(2003)115<0643:AMSIGR>2.0.CO;2.

Nishiizumi, K., Winterer, E.L., Kohl, C.P., Klien, J., Middleton, R., Lal, D., and Arnold, J.R., 1989, Cosmic ray production rates of ^{10}Be and ^{26}Al in quartz from glacially polished rocks: *Journal of Geophysical Research*, v. 94, p. 17,907–17,915.

- Oldow, J.S., 1992, Late Cenozoic displacement partitioning in the northwestern Great Basin, *in* Lane, C., and Steven, D., eds., Geological Society of Nevada Walker Lane symposium: Structure, tectonics and mineralization of the Walker Lane: Reno, Geological Society of Nevada, p. 17–52.
- Pakiser, L.C., Kane, M.F., and Jackson, W.H., 1964, Structural geology and volcanism of the Owens Valley region, California—A geophysical study: U.S. Geological Survey Professional Paper 438, 68 p.
- Peltzer, G., Crampe, F., Hensley, S., and Rosen, P., 2001, Transient strain accumulation and fault interaction in the eastern California shear zone: *Geology*, v. 29, p. 975–978, doi: 10.1130/0091-7613(2001)029<0975:TSAAFI>2.0.CO;2.
- Philip, H., and Megard, F., 1977, Structural analysis of the superficial deformation of the 1969 Pariahuanca earthquakes (central Peru): *Tectonophysics*, v. 38, p. 259–278, doi: 10.1016/0040-1951(77)90214-1.
- Philip, H., and Meghraoui, M., 1983, Structural analysis and interpretation of the surface deformations of the El Asnam earthquake of October 10, 1980: *Tectonics*, v. 2, p. 17–49.
- Phillips, F.M., Zreda, M.G., Smith, S.S., Elmore, D., Kubik, P.W., and Sharma, P., 1990, Cosmogenic chlorine-36 chronology for glacial deposits at Bloody Canyon, eastern Sierra Nevada: *Science*, v. 248, p. 1529–1532.
- Rockwell, T.K., Lindvall, S., Herzberg, M., Murbach, D., Dawson, T., and Berger, G., 2000, Paleoseismology of the Johnson Valley, Kickapoo, and Homestead Valley faults: clustering of earthquakes in the eastern California shear zone: *Bulletin of the Seismological Society of America*, v. 90, p. 1200–1236, doi: 10.1785/0119990023.
- Small, E.E., Anderson, R.S., Repka, J.L., and Finkel, R.C., 1997, Erosion rates of alpine bedrock summit surfaces deduced from in-situ Be-10 and Al-26: *Earth and Planetary Science Letters*, v. 150, p. 413–425, doi: 10.1016/S0012-821X(97)00092-7.
- Spudich, P., Mariagiovanna, G., Kenschiro, O., and Jun, M., 1998, Use of fault attritions and dislocation models to infer tectonic shear stress during the 1995 Hyogo-ken Nanbu (Kobe) earthquake: *Bulletin of the Seismological Society of America*, v. 88, p. 413–427.
- Stewart, J.H., 1988, Tectonics of the Walker Lane belt: Mesozoic and Cenozoic deformation in a zone of shear, *in* Ernst, W.G., ed., *Metamorphism and crustal evolution of the Western U.S.*, Rubey Vol. VII: New York, Prentice Hall, p. 684–713.
- Stock, G.M., Anderson, R.S., and Finkel, R.C., 2004, Pace of landscape evolution in the Sierra Nevada, California, revealed by cosmogenic dating of cave sediments: *Geology*, v. 32, p. 193–196, doi: 10.1130/G20197.1.
- Stone, J., 2000, Air pressure and cosmogenic isotope production: *Journal of Geophysical Research*, v. 105, p. 23,753–23,759, doi: 10.1029/2000JB900181.
- Thatcher, W., Foulger, B.P., Julian, B.R., Svarc, J., Quilty, E., and Bowden, G.W., 1999, Present-day deformation across the Basin and Range Province, western United States: *Science*, v. 282, p. 1,714–1,718.
- Unruh, J., Humphrey, J., and Barron, A., 2003, Transtensional model for the Sierra Nevada frontal fault system, eastern California: *Geology*, v. 31, p. 327–330, doi: 10.1130/0091-7613(2003)031<0327:TMFTSN>2.0.CO;2.
- U.S. Geological Survey, 2004, United States Geological Survey Quaternary Fault and Fold Database for the United States; Nevada, <http://earthquakes.usgs.gov/qfaults/nv/index.html>.
- Wakabayashi, J., and Sawyer, T.L., 2001, Stream incision, tectonics, uplift, and the evolution of topography of the Sierra Nevada, California: *Journal of Geology*, v. 109, p. 539–562, doi: 10.1086/321962.
- Wernicke, B., Friedrich, A.M., Niemi, N.A., Bennett, R.A., and Davis, J.L., 2000, Dynamics of plate boundary fault systems from Basin and Range Geodetic Network (BARGEN) and geologic data: *GSA Today*, v. 10, no. 10, p. 1–7.
- Wesnousky, S.G., and Jones, C.H., 1994, Oblique slip, slip partitioning, spatial and temporal changes in the regional stress field, and the relative strength of active faults in the Basin and Range, western United States: *Geology*, v. 22, p. 1031–1034, doi: 10.1130/0091-7613(1994)022<1031:OSSPSA>2.3.CO;2.
- Wesnousky, S.G., Barron, A.D., Briggs, R.W., Caskey, J.S., Kumar, S., and Owen, L., 2005, Paleoseismic transect across the northern Great Basin: *Journal of Geophysical Research*, v. 110, B05408, doi: 10.1029/2004JB003283, doi: 10.1029/2004JB003283.
- Whipple, K.X., and Dunne, T., 1992, The influence of debris-flow rheology on fan morphology, Owens Valley, California: *Geological Society of America Bulletin*, v. 104, p. 887–900, doi: 10.1130/0016-7606(1992)104<0887:TIODFR>2.3.CO;2.
- Wright, L., 1976, Late Cenozoic fault patterns and stress fields in the Great Basin and westward displacement of the Sierra Nevada block: *Geology*, v. 4, p. 489–494, doi: 10.1130/0091-7613(1976)4<489:LFCPAS>2.0.CO;2.
- Zehfuss, P.H., Bierman, P.R., Gillespie, A.R., Burke, R.A., and Caffee, M.C., 2001, Slip rates on the Fish Springs fault, Owens Valley, California, deduced from cosmogenic ¹⁰Be and ²⁶Al and soil development on fan surfaces: *Geological Society of America Bulletin*, v. 113, p. 241–255, doi: 10.1130/0016-7606(2001)113<0241:SR0TFS>2.0.CO;2.
- Zoback, M.L., 1989, State of stress and modern deformation of the Basin and Range Province: *Journal of Geophysical Research*, v. 94, p. 7105–7128.
- Zoback, M.L., and Zoback, M.D., 1989, Tectonic stress field of the continental U.S., *in* Pakiser, L., and Mooney, W., eds., *Geophysical Framework of the Continental United States*: Geological Society of America Memoir 172, p. 523–539.

MANUSCRIPT RECEIVED 26 DECEMBER 2005
 REVISED MANUSCRIPT RECEIVED 6 JUNE 2006
 MANUSCRIPT ACCEPTED 3 AUGUST 2006

Printed in the USA